Journal of Materials Chemistry A

Accepted Manuscript

This article can be cited before page numbers have been issued, to do this please use: M. Osiak, H. Geaney, E. Armstrong and C. ODwyer, *J. Mater. Chem. A*, 2014, DOI: 10.1039/C4TA00534A.

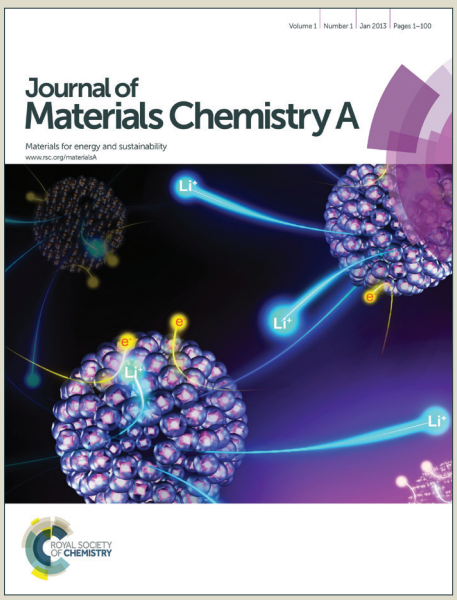

ROYAL SOCIETY OF CHEMISTRY

www.rsc.org/materialsA

View Article Online
DOI: 10.1039/C4TA00534A

Structuring Materials for Lithium-ion Batteries: Advancements in Nanomaterial Structure, Composition, and Defined Assembly on Cell Performance

Michal Osiak[1], Hugh Geaney[1,2], Eileen Armstrong[1], and Colm O'Dwyer[1,2]*

[1]*Department of Chemistry, University College Cork, Cork, Ireland*

[2]*Micro & Nanoelectronics Centre, Tyndall National Institute, Dyke Parade, Cork, Ireland*

Correspondence to: Colm O'Dwyer, Department of Chemistry, and Tyndall National Institute, University College Cork, Cork, Ireland. Tel: +353 (0)21 4902732; Fax: +353 (0)21 4274097; email: c.odwyer@ucc.ie

View Article Online
DOI: 10.1039/C4TA00534A

Abstract

This review outlines the developments in the structure, composition, size, and shape control of many important and emerging Li-ion battery materials on many length scales, and details very recent investigations on how the assembly and programmable order in energy storage materials has not only influenced and dramatically improved the performance of some Li-ion batteries, but offered new routes toward improved power densities. This review also describes and discusses materials aspects of hybrid and multiphasic materials including silicon, germanium, a wide range of metal oxides, alloys and crystal structures, carbons and other important materials. Methods where engineered porosity that offers the energy density of Li-ion batteries and the power density of pseudocapacitors are also highlighted. Recent developments in the analytical methods, electrochemical response, and the structure, composition, size, shape and defined assembly of active materials for a wide range of Li-ion cathodes and anodes are compared and assessed with respect to cell performance. Perspectives on the future development of energy storage materials based on structure as well as the chemistry is also outlined.

View Article Online
DOI: 10.1039/C4TA00534A

1. Introduction

The earliest research that can be connected to lithium-ion batteries originates in a graduate thesis written by Harris [1, 2], demonstrating the possibility of electrodepositing Li metal under controlled non-aqueous conditions. This converged with earlier studies in sodium ion transport in beta alumina [3] where ions intercalate, or insert into a crystalline lattice, or through porous one dimensional channels in some crystalline structures, or indeed between two dimensional layers in crystalline solids. In 1976, Whittingham at Exxon, reported intercalation electrodes arranged into a functioning rechargeable lithium battery [2]. Following that, in 1980s Armand introduced the rocking chair concept [4], where the conduction of Li ions can move repeatedly from one side of the battery to other, i.e. diffuse from the anode to cathode during charge and from cathode to anode during discharge. Development of materials that could undergo this process numerous times resulted first in commercialization of primary (single use) and subsequent widespread utilization of secondary Li-ion batteries (rechargeable LIBs).

Rechargeable Li-ion batteries are one of the most extensively researched power sources for applications in modern portable electronics, hybrid electrical vehicles and sensor networks, as highlighted by a number of recent review articles [5-8]. Newer consumer electronics that are developed require power sources with higher energy density (amount of energy stored per unit mass), higher power density (time rate of energy transfer), longer lifetime (the number of cycles of battery charge/discharge) and improved safety of operation. Early secondary Li-ion batteries suffered greatly from thermal instabilities caused by dendritic depositions of Li from the metallic Li anode through to the cathodes [9], leading to the formation of short circuit connections between the electrodes and in some cases ignition of the battery package when certain electrolytes were used. This problem was

View Article Online
DOI: 10.1039/C4TA00534A

overcome by replacing metallic Li anode with various non-metal compounds [10], capable of storing and reversibly exchanging large number of Li ions. The reduction of Li plating effects (and associated safety improvement) gave way to widespread introduction of Li-ion batteries into consumer markets[11]. Figure 1 presents a schematic diagram of a secondary Li-ion battery. It consists of following elements, from left to right in the image:

a) **Cathode**. The cathode is the positive electrode of the battery, which means it is the source of positive ions (Li^+) and accepts negative ions (e^-). In currently used batteries, cathodes are most commonly made of (but not limited to) layered, or spinel lithiated metal oxides.

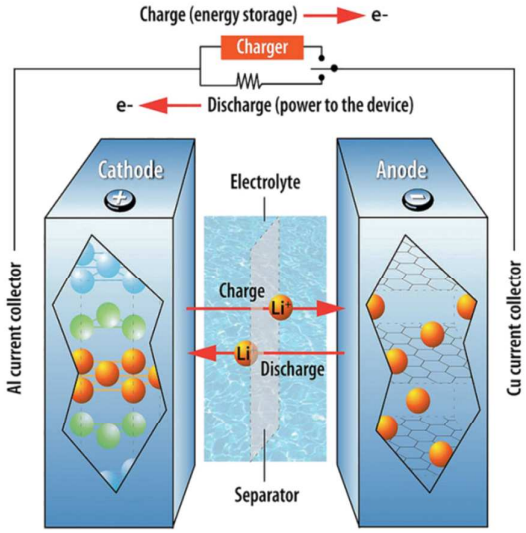

Figure 1. Structure and principle of operation of a Li ion battery.

In layered cathodes, the composition is denoted by $LiMO_2$, where M corresponds to Co [12, 13], Ni [14], Mn [15] or V [16, 17]. $LiCoO_2$ is currently the most popular option, despite the high cost of cobalt, as it is relatively easy to prepare a high quality electrode with a layered

View Article Online
DOI: 10.1039/C4TA00534A

structure of extremely high quality. This material and associated battery construct has also benefited from decades of research, development and real-world applications. Nickel manganese [18] and vanadium [19] are being extensively investigated in order to improve their structural stability, reversibility and cost-effectiveness for some applications. Spinel cathodes (e.g. $LiMn_2O_4$) offer the advantage of a robust cubic oxygen array with 3-dimensional Li ion diffusion, allowing fast insertion/removal of Li ions during discharge/charge processes[20].

b) **Electrolyte**. At high operating potentials (up to 4.5-5 V vs Li/Li^+ for some advanced cathode materials) associated with operation of Li-ion batteries, aqueous solutions would electrolyze easily if used as an electrolyte for a Li cell. Thus, aprotic, non-aqueous solvents are used [21]. Commonly used electrolytes LIBs include propylene carbonate, dimethyl-carbonate, ethylene carbonate, vinylene carbonate and mixtures of these solvents[22]. As liquid electrolytes do not fully prevent formation of dendrites on the surface of the anode, often solid state polymer electrolytes are used. The electrolyte needs to satisfy certain conditions:

- High Li ion conductivity, very low electronic conductivity
- Wide temperature range of operation
- The energy gap between the electrolyte's lowest unoccupied molecular orbital (LUMO) and highest occupied molecular orbital (HOMO) needs to be higher than the difference between energy levels of cathode and anode; it needs to be thermodynamically stable at the operating voltages.
- It should ideally be environmentally friendly.

In the electrolyte Li salts such as $LiClO_4$, $LiBF_4$, and $LiPF_6$ are dissolved to act as a source of Li^+ ions. The use of vinylene carbonate additives in some carbonate electrolytes, among others,

View Article Online
DOI: 10.1039/C4TA00534A

promotes Solid Electrolyte Interphase (SEI) formation at the anode through radical polymerization, which is beneficial for stabilizing the interface during repetitive insertion (or alloying) and removal of lithium ions [23].

c) **Separator**. The separator provides a barrier which prevents short circuiting of the cathode and anode. It should be sufficiently porous to allow the electrolyte to freely connect the two electrodes. Most commonly, separators are made of polytetrafluoroethylene (PTFE) and other inert polymer membranes with defined porosity and ionic conductivity.

d) **Anode**. The anode is the negative electrode of the Li ion battery. In currently used commercial packages, the anode consists of layered graphitic carbon. The storage mechanism is based on the intercalation of Li^+ ions into van der Walls spacings found between the graphitic monolayers. The theoretical specific capacity of graphitic carbon is 372 $mAhg^{-1}$, based on following reaction:

$$LiC_6 - e^- \leftrightarrow 6C + Li^+$$

Graphitic carbon electrodes allow for good cycle lifetime, but suffer from low rate capability, and irreversible capacity losses caused by electrolyte decomposition at low potentials, and formation of a solid electrolyte interphase (SEI). SEI is a common name given to a passivating layer formed on the surface of the electrode due to reductive decomposition of the electrolyte [24]. It forms at low potentials (typically, 0.7 V vs Li/Li^+). In the initial cycle, the formation of a SEI layer contributes to the loss of reversible capacity. However, in subsequent cycles, the SEI layer prevents additional decomposition of the electrolyte, improving reversible capacity and ensuring better cycling of the battery. To optimize electrode performance, the SEI layer should be insoluble in the electrolyte, be a good electronic insulator and ionic conductor. Importantly, the SEI layer should be able to remove

View Article Online
DOI: 10.1039/C4TA00534A

a thin solvation layer around the Li^+ ion, to prevent the exfoliation or delamination of layered active material that could result from by co-intercalation of the solvent [25-28].

Battery research is driven by the economical need to satisfy consumer demand for higher power and higher energy batteries. Every smartphone user would like to see their phone operate for a prolonged period of time under high demand usage. Global climate change makes the prospect of all-electrical cars a welcome alternative to petrol, gas or diesel-fuelled transport. The "always on, always connected society" with strong demands on wireless sensor networks will require more advanced power solutions than those currently available, in smaller volumes with long term stability for operation in remote locations. So far, many possible replacement materials have been identified for both anode and cathode, and require even more development for any non-lithium based electrochemical power sources. Moreover, the advent of nanotechnology has facilitated battery architectures which are no longer entirely reliant on traditional bulk/thin film approaches, but with structurally engineered porous, 1, 2 or 3 dimensional designs offering improvements in performance [6, 29, 30]. This review will describe some of the most recent findings in both the structural design and the materials chemistry of next generation battery electrodes.

2. Choosing materials for Li-ion batteries

As mentioned above, novel materials for Li-ion batteries have been extensively investigated over a number of years. Several materials have been identified as potential replacements of cathode and anode in next generation battery anodes (summarised in Figure 1), and have been in some cases commercialized, demonstrating great potential for currently researched materials. However, before wide-scale adaptation of new materials, a deeper and better

View Article Online
DOI: 10.1039/C4TA00534A

understanding of all the factors affecting battery performance (its chemistry, upscaling, packaging and drivetrain) needs to be developed. Many excellent reviews provide details of material performance, and their performance and fundamental response as lithium-battery electrode materials and the reader is referred to other reviews for selected ranges of materials [5, 7, 8, 31, 32].

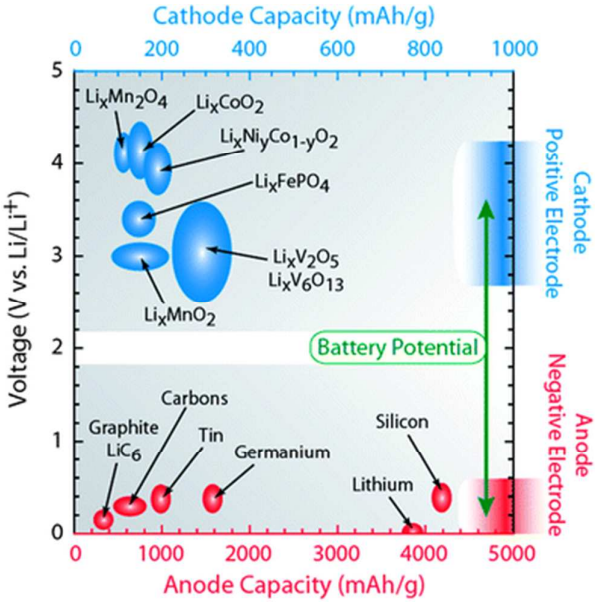

Figure 2. Diagram illustrating the Li ion capacity and electrochemical reduction potentials with respect to Li metal for a range of cathode and anode materials [11].

A pioneering method for materials choice and for future development is being developed by Ceder et al. at MIT, using what they term the *Materials Genome Project* [33]. The Materials Genome Project has a goal of applying knowledge gained from large-scale property computation on all known inorganic compounds for materials research and discovery. While applicable to many functional applications involving materials whose properties would ideally like to be predicted, it has immediate useful application to Li-ion and emerging alternative battery chemistries. Many tens of thousands of materials have

View Article Online
DOI: 10.1039/C4TA00534A

been screened in terms of Li^+ intercalation voltage or chemical potential, theoretical charge capacity, electrode voltage and other parameters. Figure 3 shows the voltage calculated using density functional theory as a function of the theoretical capacity for thousands of oxides, phosphates, borates, silicates, and sulfates. The continuing work is also focused on the safety of high voltage materials is various electrolytes and structural effects that are related to cycling behaviour and performance.[34] It forms a new and extremely useful approach to Li-ion battery materials design.

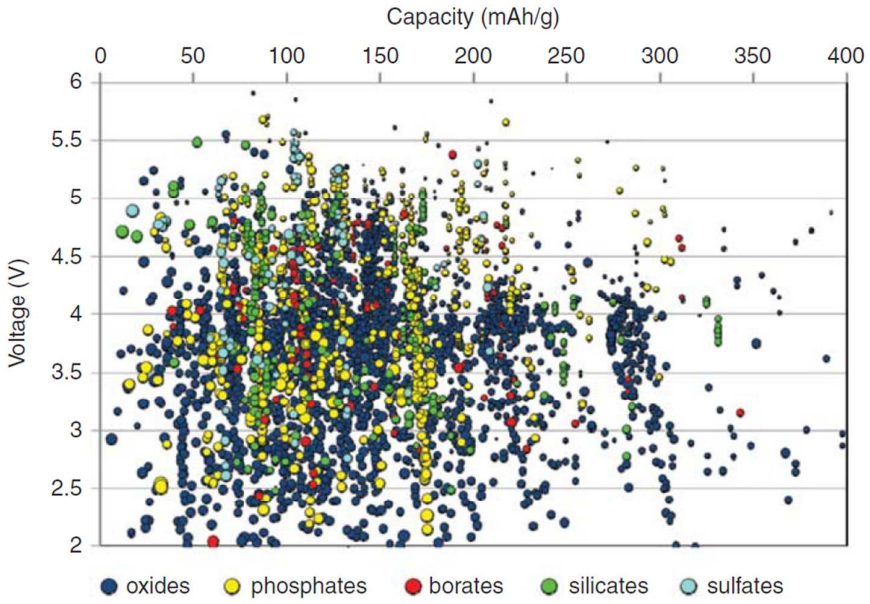

Figure 3. Calculated lithium insertion voltage versus theoretical capacity for several thousand compounds. Reproduced from [35] with permission form the Materials Research Society.

In general, next-generation Li-ion battery materials can be divided into sub-categories based on their Li^+ ion storage mechanism: intercalation electrodes, conversion electrodes and alloying electrodes.

View Article Online
DOI: 10.1039/C4TA00534A

3. Intercalation Electrodes

Intercalation electrodes involve materials with crystalline structure enabling diffusion of Li ions into the interstitial sites of the crystalline lattice. The most common crystalline structures include layered [36], olivine [37, 38] and spinel [39] (Figure 4). Their main appeal lies in their excellent structural stability and long cycle lifetime. Currently used cathodes consist of layered $LiCoO_2$, $LiCo_{1-y}Ni_yO_2$ and $LiMn_2O_4$. These cathode materials have some practical limitations however. $LiCoO_2$ can only intercalate in the $LiCoO_2$ – $Li_{0.5}CoO_2$ range, limiting available capacity to about 130 $mAhg^{-1}$. Cheaper and more environmentally friendly $LiCo_{1-y}Ni_yO_2$ suffers from strong Li-Ni cation mixing, which affects the structure formation and subsequent ionic transport. $LiMn_2O_4$ in turn has a limited stability and may undergo phase transition at room temperature [40]. Further computational investigations showed however, that the addition of some nickel, to form $Li(Mn_{0.5}Ni_{0.5})O_2$, yields an almost ideal cathode material in theory, due to the stability of the closed-packed framework of Mn^{4+} coordinated to oxygen [41]. However, the rate capability for this material was very poor and the mobility of Li ions within the framework was found to be strongly linked to the distance between the oxygen layers.

For battery safety, particularly at high deintercalation rates or under typical discharge/charge at elevated temperatures, self-catalysed exothermic reactions of the active material with the electrolyte may occur [42], leading to thermal instabilities, thermal runaway and ultimately a failure (and sometimes explosion) of the battery. Recent reports of fires caused by exploding LIBs are an example of a result of instabilities arising from the interaction of the highly charged cathode with the electrolyte, often aided and sometimes facilitated by electrical shorting from Li dendrite formation [43]. Cathode materials with inherently active or unstable oxidation states can potentially be reduced by liberating

View Article Online
DOI: 10.1039/C4TA00534A

oxygen, which overcomes its kinetic limitations at elevated temperatures cause by heat from surrounding environment or possibly by self-discharge and cell heating. The oxygen can vigorously react and burn the electrolyte. However, there are many materials (cathode materials) that have a large negative chemical potential (difficult to reduce in their charged state) and thus are inherently safe in this regard, $LiFePO_4$ being cited as possibly the ideal example. Interestingly, and widely known, is that the most prevalent battery chemistry employing $LiCoO_2$ is inherently one of the least safe in its charged state, but does offer good cycling capability. Advances in the engineering of battery packs has largely removed these issues, but several high profile accidents have reignited the issue of battery safety and raise the question of safer chemistries by choosing safer electrolytes or electrode materials [44].

Layered and spinel materials however suffer from low Li ion diffusivity, and therefore can only satisfy limited power demands. In recent years, research has been mainly focused on improving the electrode kinetics [45-47]. Nanostructuring active material offers significant benefits, such as: shortened diffusion lengths, improving electrical and ionic performance/rate by placing conductive additives as a surface coating on active materials, as opposed to a random mixture of powder additives [48, 49]. Some of the various nanostructures formed include, but are not limited to, nanosheets [50], nanoparticles [51], nanowires [52] and nanotubes [53].

View Article Online
DOI: 10.1039/C4TA00534A

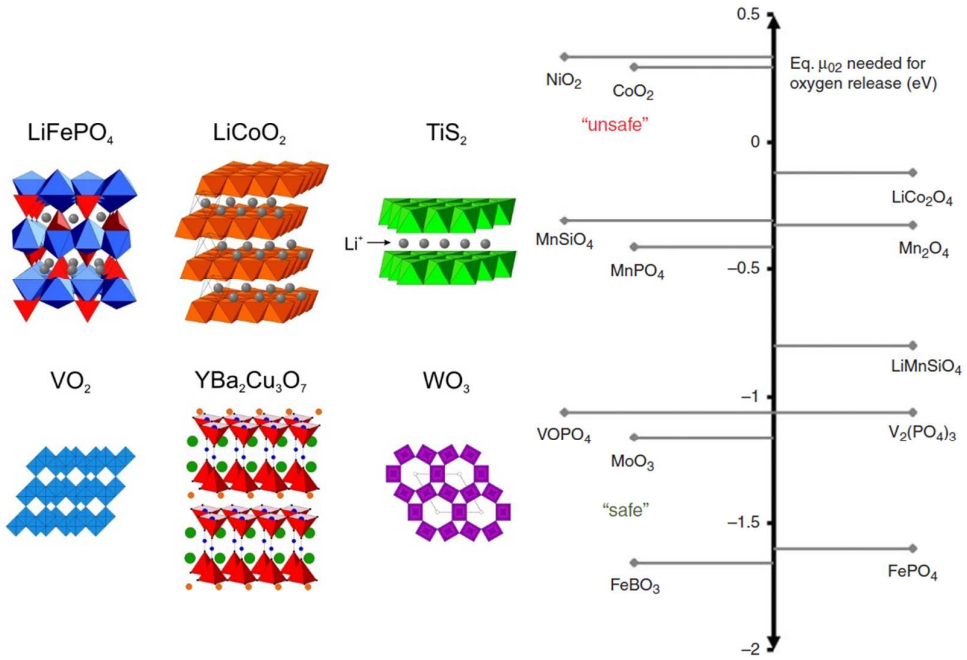

Figure 4. (a) A range of different oxide, sulfide and phosphate crystal structures capable of Li intercalation to various regions of their crystal structure Reproduced from [54] with permission from Intech Open. (b) Common intercalation compounds as a function of decreasing calculated chemical potential of oxygen in their charged state. A lower oxygen chemical potential is deemed safer. Reproduced from [35] with permission from the Materials Research Society.

4. Conversion materials

A different type of Li storage mechanism is a reversible electrochemical reaction of Li with transition metal oxides [55, 56]. The mechanism of the energy storage is conventionally referred to as conversion reaction, described as follows:

$$M_aX_b + (b \cdot n)Li \leftrightarrow aM + bLi_nX$$

where M = transition metal, X = anion and n is the formal oxidation state of X. Conversion reactions have been reported for some oxides, sulfides and fluorides, with different degrees of reversibility. The main focus of researchers working with conversion based electrodes is the improvement of electrode kinetics and reversibility, in particular, formation of

View Article Online
DOI: 10.1039/C4TA00534A

nanoparticles of reduced metals that would be very active towards the Li_nX matrix in which they are interspersed. At the moment, however, conversion type electrodes are still in development, and much investigation is required into fundamental characteristics of conversion materials and electrode design.

5. Alloying materials

Reversible electrochemical alloying of metals and semi-metals with Li has been known since 1970s [57]. Metals reversibly alloying with Li offer tremendous improvement in specific Li storage capacity. Silicon has a highest known theoretical Li storage capacity, higher even than that of Li (3700 $mAhg^{-1}$) equal to 4400 $mAhg^{-1}$ [6]. Other examples of alloying materials include tin and tin oxides [58], antimony [59], germanium [60], and others like phosphorus, magnesium and silver [7], each offering excellent theoretical Li storage capacity. However, these materials suffer greatly from large volumetric expansion and contraction caused by insertion and removal of a large amount of Li^+ ions, as well as fast charging/discharging rates. Severe mechanical stresses and strains resulting from repeated cycles of volume changes lead to irreversible structural changes, formation of cracks in active material causing loss of structural and electrical integrity of the electrode, pulverization and irreversible capacity fading. The most common strategies directed at the improvement of electrode performance are focused on the accommodation of volumetric expansion through providing free space around the active material [5] and creating various composites [61-64] aimed at protection of the active material against structural degredation or ensuring consistent and stable electrical contact between the active material and external current collector.

View Article Online
DOI: 10.1039/C4TA00534A

The scope of this section is to summarise recent advances in the field of alloying materials research, with improved characteristics for next generation Li-Ion battery anodes.

5.1 Silicon

Silicon has for a long time been investigated as a possible replacement for graphitic carbon in next generation anode materials. In terms of specific capacity, Li-Si alloy phase can store >4000 $mAhg^{-1}$, compared to 372 $mAhg^{-1}$ for graphitic carbon. Silicon is also the second most abundant material in the earth's crust, making it economically viable for mass production of LIBs [65]. The abundance of the element, combined with the benefits of well-developed industrial infrastructure and exceptionally high theoretical specific capacity, has made Si one of the most promising materials for next generation battery anodes. However, the large number of Li ions that can be inserted into Si cause extremely large volumetric changes: $\sim V_f = 3V_i$ where *f* and *i* denote final and initial volume of the material. Mechanical failure often follows, leading to irreversible capacity loss and decrease in cycle lifetime, effectively preventing successful application of Si in next generation battery anodes.

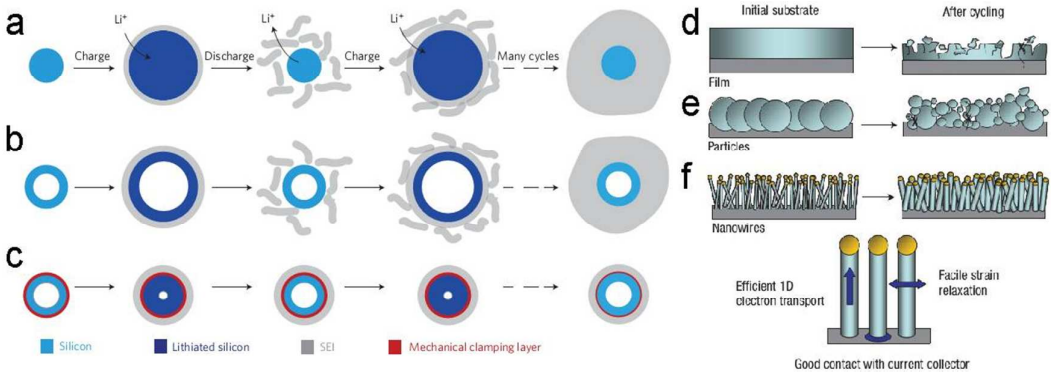

Figure 5. (a-c) Schematics of SEI layer formation and stable cycling of double-walled SiO_2@Si nanotubes. Reproduced from [66] with permission from Nature Publishing Group. Schematic changes occurring in (d) Si thin film. (e) Si nanoparticles. (f) Si nanowires. Adapted from [67] with permission from Nature Publishing Group.

View Article Online
DOI: 10.1039/C4TA00534A

Si nanostructures such as nanowires and nanoparticles have been designed and fabricated through numerous routes [6, 68]. Additionally, some nanostructures have been specifically engineered in order to accommodate the volume changes occurring in Si, such as core shell nanotubes [66] and yolk-shell type nanoparticles [69]. Figure 5 demonstrates improvements in structural stability of nanostructured Si electrode materials.

Widespread research into formation of Si NWs and their application in electrochemical energy storage, allowed better insight in the processes occurring during lithiation, and in particular structural changes caused by formation of reversible alloying of Li with Si. In-situ TEM observations indicated preferential anisotropic swelling of <112> Si nanowires in <110> direction [70]. The Li^+ diffusion study revealed deformation followed by a build-up of tensile stress in the nanowires, resulting in fracture [71]. Numerical modelling indicated that Li^+ ions prefer to diffuse along <110> direction, where surface energy of the planes is preferable for Li^+ interactions. The electrochemical lithiation of crystalline silicon leads to formation of a core-shell structure, with Li-rich amorphous Li_xSi alloy forming the shell, and crystalline silicon forming the core. The formation of the interface between the amorphous and crystalline phases is related to the stress induced Li^+ diffusion retardation, and may lead to the local loss of mechanical integrity due to large stress build-up at the interface [72, 73].

One-dimensional (1D) nanostructures were first described for use in Li-ion anodes in a seminal paper published in 2008 by Chan et al. [67], and similar studies published around the same time period [74, 75] where Si NWs were applied as anodes. Chan et al. prepared Si NWs directly on a stainless steel current collector, by gold-seeded chemical vapour deposition

View Article Online
DOI: 10.1039/C4TA00534A

(CVD). The nature of the synthesis resulted in excellent adhesion of the active material to the substrate and in significant porosity of the electrode. Constraining the volumetric expansion through the design of the electrode morphology (Figure 5) resulted in significant improvements in electrochemical performance of the Si based electrodes. The Si nanowire arrays displayed a capacity of > 2100 $mAhg^{-1}$ at a C/20 rate, without large decrease in reversible capacity and change in the morphology of the nanowires.

Despite the promise of these CVD grown Si NWs for LIB applications, typically used gold catalysts have recently been shown to be detrimental to the electrochemical performance (in terms of initial capacity, capacity retention and rate capability) of NW based electrodes. Furthermore, Au is costly, shows poor lithium activity and is much denser than Si which strongly impacts the gravimetric capacity for a given total anode [76]. To circumvent these issues presented by the Au catalyst, recent approaches have been developed to prepare NWs through different routes, such as high boiling point solvent syntheses using electrochemically active catalyst materials such as Sn [77, 78] or shifting the grown method entirely to a metal assisted chemical etching regime.[79]

Composite Si nanostructures have also been proposed in order to improve the electrochemical performance. By incorporating the nanoscale Si inside an elastically deformable conductive host the stress changes the cause mechanical breakdown associated with electrochemical lithiation can be better accommodated, while also providing robust electronic conduction pathways.

A different approach to improving the electrochemical performance of the Si based LIBs is preparing Si-C composites. Two strategies for preparing Si-C composites have been widely employed. Carbon structures such as nanotubes, nanosheets of graphene or carbon

View Article Online
DOI: 10.1039/C4TA00534A

fibres have been used as supports for nanoscale active material [80-83]. By providing continuous electrical pathway from the active material to the current collector, the influence of the electrochemically induced agglomeration of the nanoparticles on the electrochemical performance is greatly reduced. Moreover, using carbon support offers excellent porosity allowing for better penetration of electrolyte throughout the electrode, shortening diffusion lengths, allowing for higher rates of charge/discharge, summarised in Figure 6.

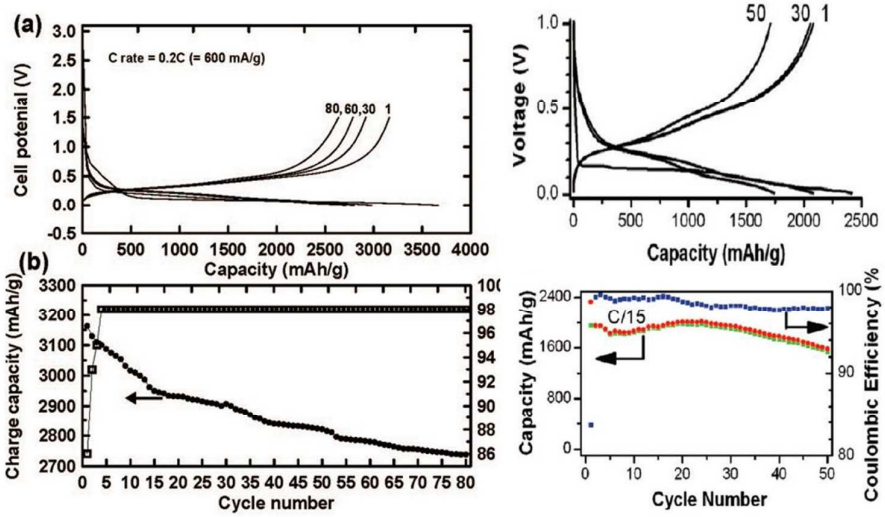

Figure 6. Constant current line-sweeps and cyclic performance for a) carbon coated. Reproduced from [84] with permission from the American Chemical Society. b) Carbon supported Si nanostructures. Reproduced from [85] with permission from the American Chemical Society.

In contrast to the supported electrodes, carbon coatings are a different strategy for preparing carbon composites with Si [86-89]. By applying a thin (few to few tens to at most few tens of nanometres) coatings of carbon on the surface material, a mechanically stable layer that can provide support to the nanostructures, and thus preserve their mechanical integrity during repeated charge-discharge cycles, can be formed. Additionally, the continuous layer present on the surface of the active alloying material acts as a stable conductor from the

View Article Online
DOI: 10.1039/C4TA00534A

electrode to the current collector. An extension of this strategy is the preparation of composites in which nanostructures of alloying materials are embedded in a carbonaceous matrix. Carbon forms a stable SEI layer with the species present in the electrolyte, and has been shown to provides a degree of mechanical support against rapid expansion and contraction during electrochemical cycling in randomly mixed slurries, but also in 3D ordered porous materials with electrochemically active materials embedded within the carbon matrix [90]. The problems arising from this approach are mostly related to low ionic conductivity of carbonaceous matrix and resulting low rate capability of such prepared nanostructures.

Within a vast multitude of structures prepared for Si based anodes, nanotubes seem to offer the best electrochemical performance, due to the mechanisms of Si lithiation, and free space provided for volumetric expansion of the nanostructures. To alleviate the repeated re-formation of SEI layer, electrochemically-inactive SiO_2 layer was used in order to ensure SEI layer stability. The mechanical robustness of SiO_2 provides buffering against stress induced cracking within the nanotubes, while ensuring formation of a stable SEI layer. To date, SiO_2@Si nanotubes show one the best electrochemical performance for Si based anodes [66] (see Figure 5). The need to commercialize Si based batteries will undoubtedly result in further improvements in the Si based LIB performance.

Table 1 presents comparison between some of recently prepared Si based materials for LIB anodes.

Composition	Morphology	Initial Capacity (C-rate)	Final Capacity (# cycles)	Reference
Si	NWs	4277 (C/20)	3500 (20)	[67]
Si@SiO_x/C	NPs	1600	1100 (60)	[91]
Si@C	Mesoporous CS NWs	3163C/5	2751 (80)	[84]
Si	3D Porous	2820 (C/5)	2780 (100)	[92]
C-Si	Core-shell NWs	700 (C/15)	1600 (47)	[93]

View Article Online
DOI: 10.1039/C4TA00534A

Si-C	Carbon coated NWs	3344	1326(40)	[94]
Si	Nanotubes	3648 (C/5)	2800 (200)	[95]
Si-Graphene	Composite	2158 (C)	1168 (30)	[96]
Si-CNT	Composite	2300 (C/10)	1400 (50)	[85]
Si	NWs	4000 (C/10)	1600 (50)	[97]
Si/C	Nanocomposite	2000(C/20)	1700 (100)	[98]
Si	Nanotubes	3200 (C/20)	2800 (50)	[99]
Cu-Si	Nanocables	1500 (C/3)	1400 (100)	[100]
B-doped Si	NWs	3354 (C/10)	1500 (250)	[101]
SiO_2@Si	Nanotubes	1780(C/5)	1600 (2000)	[66]

Table 1. Summary of the relative performance of different Si based electrodes.

5.2 Germanium

Germanium can also store Li through similar alloying reactions to those associated with Si. Fully lithiated $Li_{4.4}Ge$ has a high theoretical capacity of 1600 $mAhg^{-1}$ [60]. Similarly, large amounts of Li atoms stored in Ge, cause it to expand and contract upon cycling, with volume changes reaching 370% [60]. One very exciting property of Ge based anodes is the fact that Li diffusivity in Ge is 400 times greater than in Si, indicating that Ge may be an attractive material for high-power rate anodes [102, 103]. Additionally, the electrical conductivity of Ge is about 4 orders of magnitude higher than Si. Initial investigation into thin films of Ge showed that crystalline Ge suffers from large irreversible capacity loss during initial cycles. In contrast, amorphous and nanocrystalline films of Ge show greater capacity retention, with capacities as high as 1700 $mAhg^{-1}$ reported after over 60 cycles (see Figure 7 a). Shortened diffusion lengths also allowed for much improved kinetics of the Li insertion and removal, permitting charge/discharge rates as high as 1000 C with little capacity loss[102] (Figure 7).

View Article Online
DOI: 10.1039/C4TA00534A

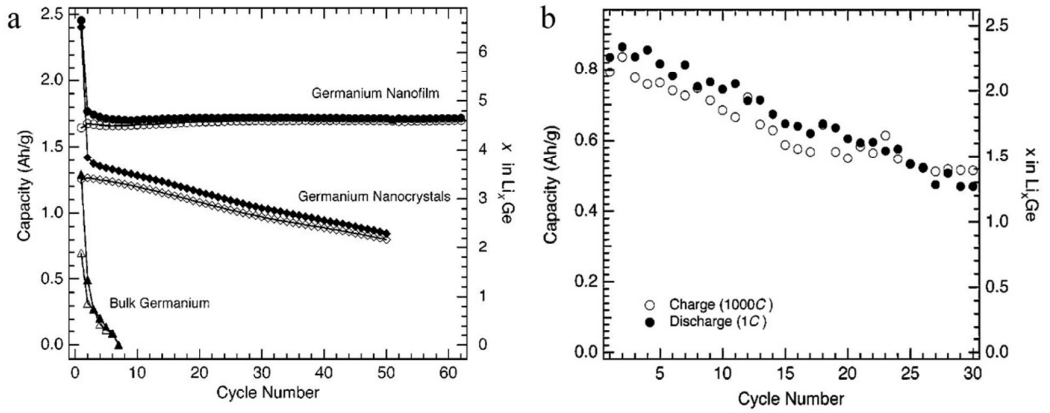

Figure 7. (a) Cycle life of Ge nanocrystals. (b) Cycle life of thin film Ge at 1000 C charge and 1 C discharge. Reproduced from [102] with permission from The Electrochemical Society.

A variety of nanostructures have been prepared in order to further improve the performance of Ge based electrodes [60, 104-107]. For instance, Au-seeded Ge nanowires prepared by CVD showed high capacities of over 850 $mAhg^{-1}$ at C/20 rates, and were able to deliver more than 600 $mAhg^{-1}$ at 2C rates. Effects arising from incorporation of Au into the nanowire (given the aforementioned issues stated in the last section) during growth however remain a problem [76].

In another example, Park et al [107], used the Kirkendall effect to prepare Ge nanotubes from core-shell Ge-Sb nanowires. Coating with antimony (Sb) acetate and polyvinyl pyrrolidone was followed by high temperature annealing. As outward diffusion of Ge atoms is much faster than inward diffusion of antimony, void formation begins in places where Ge atoms us to reside. Prolonged thermal treatment allows for the formation of amorphous nanotubular structures of Ge, with very low concentration of Sb. The unique structure of the nanotubes permitted facile accommodation of mechanical stresses and improved cycle

View Article Online
DOI: 10.1039/C4TA00534A

performance, with capacities as high as 900 $mAhg^{-1}$ after 50 cycles at C/5, and 600 $mAhg^{1}$ after 25 cycles at 20C.

In composite electrode materials, the use of carbon with Ge results in more stable electrodes, which has been evidenced by an improvement in electrochemical properties. The Ge-C composite can also reduce the degree of mechanical failure arising from multiple cycling. One effective strategy is the dispersion of nanosized material into a carbon matrix, where carbon acts as both structural buffer and electro-active material during Li incorporation/extraction. Cui et al. [104] prepared Ge nanoparticles encapsulated with carbon, through solid state pyrolysis of PTA-Ge, thermally polymerized from tetraallylgermane (TA-Ge). Initial discharge and charge capacities of 1190 and 923 $mAhg^{-1}$, and low capacity fading confirmed the effectiveness of the carbon matrix in improving the electrochemical performance of the Ge nanostructures. Carbon coating is another effective strategy to improve performance. For example, Yoon et al. prepared carbon coated Ge composites by high energy ball-milling of commercial Ge powders and poly(vinyl alcohol) (PVA)[108], producing carbon coated composites with good high initial capacities of up to 1600 $mAhg^{-1}$ and good capacity retention for up to 50 cycles. A variety of other reports was also produced detailing preparation and characteristics of Ge-C composites, including formation of core shell Ge@C nanoparticles [109], self-assembled Ge/C nanostructures [110], graphene-supported Ge [111], or carbon coated Ge nanowires [112].

Multiple element composites are also being researched for alternative anode materials based on Ge. $Ge/Cu_3Ge/C$ composites [113] were prepared by pyrolysis and high energy mechanical milling, showing improved performance compared to Ge on its own, or Ge/C composite. The improvement in electrochemical performance was attributed to the

View Article Online
DOI: 10.1039/C4TA00534A

presence of inactive Cu as well as the carbon matrix. Cu was used also in core-shell nanowire arrays [114]. Hierarchical structures of these types of anodes have great advantages for electrochemical performance of the battery, allowing for up to 80% Coulombic efficiencies in the initial discharge as well as over 1400 mAg^{-1} after 40 cycles. The excellent properties of such anodes are attributed to unperturbed electrical contact of the current collector with the electrochemically active material, as well as large porosity of the Ge/Cu anodes.

Significant efforts dedicated to improvement of Ge based anodes show that Ge is a promising candidate for next generation LIBs. Further work is however required to fully utilize its potential, in particular to improve mechanical stability of the electrode. Moreover, ensuring formation of stable SEI layer should contribute to the overall cycling performance of Ge-based anodes in appropriate electrolytes.

5.3 Tin and tin oxide

Tin and its oxides have also attracted significant research attention due to their ability to alloy with Li. Their low cost combined with high theoretical capacities, equal to 980 $mAhg^{-1}$ for tin, 864 $mAhg^{-1}$ for tin (II) oxide, and 780 $mAhg^{-1}$ for tin (IV) oxide, make these materials a very attractive prospects for future generation Li ion batteries. However, their implementation has been hindered by the comparable volumetric expansion and contraction experienced by Sn and other alloying materials. As was the case for Si and Ge, many efforts have been undertaken in order to improve the electrochemical performance of Sn and tin oxides based batteries.

Research on tin and tin oxides for application in battery anodes dates back to two papers published in 1997 by Dahn et al. [115] and Idota et al. [116] detailing structural changes

View Article Online
DOI: 10.1039/C4TA00534A

and electrochemical properties of tin oxide based anodes. Since then, most of the research has focused on determining fundamental properties of the lithiation of tin oxide, with some interesting results, and improvement of cycle life and rate capacity. Investigations into the origin of large irreversible capacity in tin oxide anodes, causes of agglomeration of tin nanostructures upon repeated cycling as well as formation and stability of SEI layer allowed better insight into the fundamental processes in Sn-based anodes. Relatively few studies focus on the performance of metallic Sn, rather looking at SnO_2. The half-cell insertion reaction, corresponding to lithiation of SnO_2 depends on electrochemical reduction of SnO_2 to metallic Sn. The overall reaction can be written as follows:

$$SnO_2 + 4Li^+ + 4e^- \rightarrow Sn + 2Li_2O$$

$$Sn + xLi^+ + xe^- \leftrightarrow Li_xSn\ (0 < x < 4.4)$$

The reduction of SnO_2 to metallic tin is generally considered irreversible, and leads to large capacity loss in the first cycle, when the associated charge for that process is factored into the coulometric response of an alloying system [115]. Moreover, the electrode undergoes an electrochemically driven solid state amorphization process. Examination of individual nanowire-type structures, reproduced in Figure 8, has shown that during lithiation, SnO_2 nanowires elongate by about 60% axially and widen by 35% radially to accommodate the volume changes [117]. These changes are associated with a wire with a certain crystal orientation, and are likely linked to the rate of insertion/alloying at different facets, or possibly from preferential and confined axial electronic transport in tandem with preferential ionic transport to the NW walls [118].

View Article Online
DOI: 10.1039/C4TA00534A

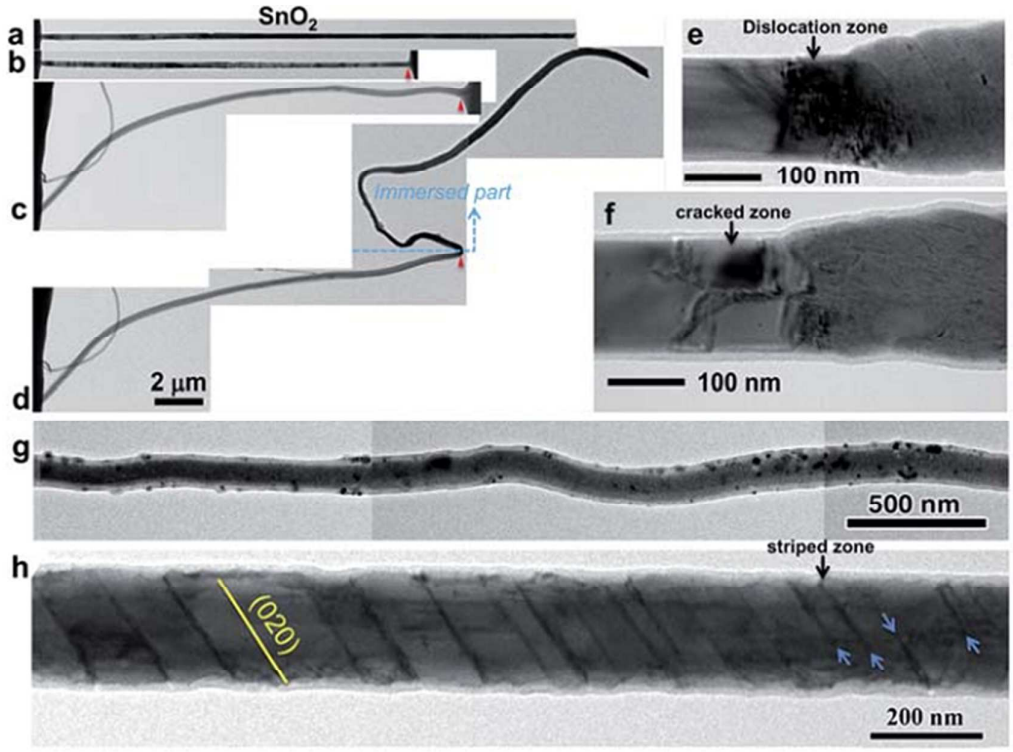

Figure 8. In situ TEM observation of the lithiation process of SnO_2 NW. Reproduced from [117] with permission from Royal Society of Chemistry.

These types of informative single-structure measurements serve to demonstrate that low- or confined-dimensional structures undergo anisotropic volume increases, but it has yet to be determined whether these effects are from the isotropy in the measurement and from the innate anisotropy of the structure and its crystallography with respect to Li diffusion and associated alloying processes.

Li insertion into crystalline SnO_2 leads to dense dislocation zones forming at the interface, separating crystalline oxide and amorphous Li-Sn phases. The nanowire morphology allows for accommodation of large degrees of strain and stress, but repeated cycling of the nanostructures may lead to pulverization and loss of mechanical integrity.

View Article Online
DOI: 10.1039/C4TA00534A

In order to improve the electrochemical performance of Sn anodes, similar strategies to those applied in Si and Ge were employed. Both nanostructuring and preparing material composites yielded some interesting results [58, 119]. Tin oxide nanostructures such as nanoparticles[120], nanowires, nanotubes all have benefits contributing to better performance of the battery electrode. In one study [121], heterostructures of indium oxide and tin oxide were prepared by thermal evaporation. Tin oxide nanowires grew with indium oxide adsorbed onto the surface of the nanowire, forming a surrounding shell. This unique concept allowed for better conductivity of SnO_2 NWs and high specific capacity, compared to SnO_2 and In_2O_3 NWs on their own. Even though nanostructuring of the electrodes has its benefits, the problem of reduced capacity due to cracking, pulverization and agglomeration of nanostructures remains. In order to further reduce the influence of physical changes on the overall performance of the battery, nanostructured composites are extensively investigated with some very exciting results. For example, core shell tin oxide-multi wall carbon nanotubes (MWCNTs) composites were prepared by hydrolysis of $SnCl_2$ in presence of HCl [122]. The excellent electrochemical performance was attributed to nanostructuring resulting in shortening diffusion lengths for Li ions, as well as the presence of MWCNT, which greatly improved conductivity of the electrode, capacity retention and Coulombic efficiency, through increased mechanical stability and persistent conduction pathways.

Tin oxide composites with other materials are also of great interest.[123-136] The benefit of using materials that are not electrochemically active, or do not undergo drastic changes has been shown in numerous studies. Materials such as copper [130, 133] nickel [137], sulphur [131], cobalt oxide [138], or titania were confirmed to benefit the performance of the battery. Copper and nickel are mainly used as support for electrochemically active tin oxide. Generally, the benefits of the electrochemically inactive electrode support allows for large

View Article Online
DOI: 10.1039/C4TA00534A

improvements in capacity retention, due to conserved electrical continuity between the active material and the current collector. However, addition of this "dead weight" material (which does not add to capacity but adds weight to the anode) may reduce the gravimetric capacity of the electrode below the capacities achieved in pristine films, so care needs to be taken to ensure that the gravimetric energy density is not lower than the electrodes composed of solely active materials. The overall capacity of composite batteries will be however limited by the combined performance of both positive (cathodes) and negative (anode) electrodes.

At the moment, cathode chemistry can limit the maximum capacity obtainable by a battery and thus, using negative electrode materials with capacities lower than the theoretical limits may be beneficial, in particular in situations where rate capability and cycle life are important. Active/inactive composites may benefit in those situations, as the active coating thickness is usually quite low, similar to the diffusion length of Li ions and so insertion and removal of ions may be extremely fast. Material such as CoO [138] form polymer like structures preventing agglomeration of tin oxide nanoparticles and improving diffusion kinetics of Li ions, improving capacity retention and rate performance (Figure 9).

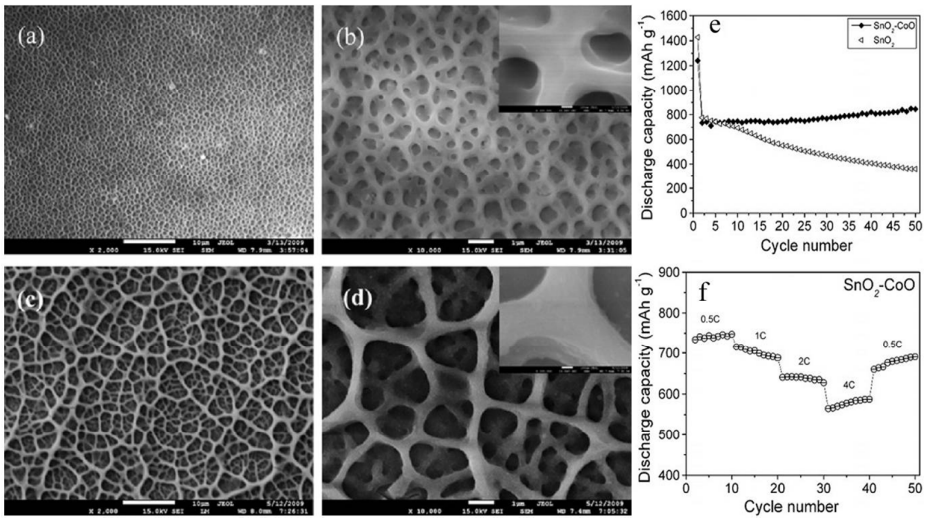

View Article Online
DOI: 10.1039/C4TA00534A

Figure 9. (a-d) SEM images of CoO-Sn; (e) Cycle performance of CO-Sn composite. (f) Rate performance of CoO composite. Reproduced from [138] with permission the Royal Society of Chemistry.

In an alternative approach, active-active composites improve the performance of the batteries, without the gravimetric density reduction penalty associated with active-inactive composite. Previously mentioned carbon-tin/tin oxide composites are included in this class of battery architectures. Other materials used in conjunction with tin are titanium oxide and cobalt. Dahn et al [139] prepared a library of Sn-Co-C composites, indicating that only a narrow composition range favours amorphous phase formation, beneficial for extended electrochemical cycling. Kim et al. [140] developed a method to prepare a nanocomposite of Sn and Ge, with improved capacity retention compared to pristine Sn and Ge. The improvements in capacity retention were attributed to the separation of Ge nanoparticles during lithiation/delithiation cycles and resulting formation of conduction pathways. The nature of the nanocomposite results however in a substantial degree of surface reactions, such as electrolyte decomposition and Li carbonate formation, resulting in unwanted contributions to irreversible capacity and internal resistance, among other effects. In cases where large surface area nanostructures are used, it is particularly important to understand the reactions taking place at the SEI. It has also been suggested that tin, formed by the reduction of tin oxide during electrochemical reactions, may contribute to large capacity fading, not due to agglomeration of nanoparticles, but due to Sn-catalyzed electrolyte decomposition [141]. In particular, this phenomenon is favoured at high current densities, where enough thermal energy is provided to accelerate diffusion of Sn, driven by desire to reduce interfacial energy. Figure 10 shows a schematic diagram of the self-catalyzed agglomeration of Sn nanoparticles.

View Article Online
DOI: 10.1039/C4TA00534A

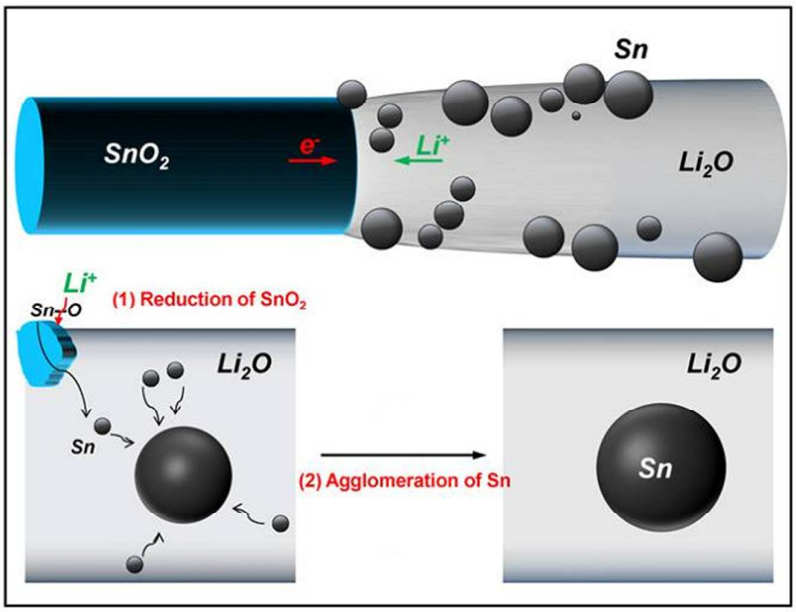

Figure 10. Schematic diagram detailing formation and aggregation of Sn nanoparticles. Reproduced from [60] with permission from American Chemical Society.

Composition	Morphology	Initial Capacity	Final Capacity	Ref
SnO_2-In_2O_3	NWs	2000 (C/5)	780 (10)	121
SnO_2- SWCNT	Composite	1399	1000 (100)	142
SnO_2-MWCNT	Composite	1500 (C/10)	404 (20)	143
Sn-Co-C	Composite	451 (C/8)	486 (40)	126
Sn-C	Composite	600 (C/8)	311 (200)	144
Sn-Co	Composite	1200 (C/2)	845 (50)	138
SnO_2 –C	GNS-NP Composite	1800 (C/15)	570 (30)	145
Sn-C	Composite	806 (C/10)	737 (200)	146
Sn-Au	Composite	1200 (C/10)	600 (150)	147
SnO_2 – C	CNT composite	1466(C/5)	402 (100)	122
SnO_2	Nanocrystal	2156 (C/10)	550 (20)	148

View Article Online
DOI: 10.1039/C4TA00534A

Sn-SnO_2	NWs	2400 (C/8)	845 (100[149])	[149]
SnO_2 –C	NPs	1200 (C/2)	492 (100)	[150]
SnO_2	Mesoporous	960 (C/6)	600 (100)	[151]
Sn-C	Nano Sn-Hard Carbo	580	300 (30)	[152]
SnO_2	Mesoporous - NW	1400 (C/5)	675 (50)	[153]
SnO_2	Nanosheets	1860 (C/10)	593 (20)	[154]
Sn-C	3D porous	1425 (C/20)	638 (315)	[155]
Sn-C	RGO-Sn	1572 (C/8)	710 (50)	[156]
SnO_2-C	Graphene Composite	1100 (C/8)	872 (200)	[62]

Table 2. Summary of the performances of different Sn and SnO_2 based elecrodes. The C rate and the cycle numbers are indicated in brackets.

Recently, Sony has commercialised its Nexelion [157] range of Li-ion cells containing anodes consisting of Sn-Co-C. Such alloys have shown excellent cycling abilities attributed to active-inactive relationship between Sn and Co [124, 126]. Other alloys including active-inactive system are Sn-Ni-C and Sn-Cu. The Nexelion device demonstrates improved capacity and cycling performance compared to traditional carbon based batteries. In a study carried out by the Army Research Laboratory [158], Nexelion batteries showed good performance at elevated temperatures, and stability at high discharge rates. Although, as the study notes, cycle-to-cycle capacity retention of the Nexelion is slightly worse than standard 14430 cell, its increased initial capacity allows it to retain higher reversible capacity after 220 cycles. The commercial utilisation of Sn has demonstrated its purposeful character as battery anode material in cost effective and efficient manner. Table 2 details the

View Article Online
DOI: 10.1039/C4TA00534A

electrochemical performance of a variety of recently prepared SnO_2 nanostructures which further highlights the promise of Sn and Sn composite based materials as low cost, high performance anode materials.

6. Role of electrode structure on electrochemical performance

The previous section of this review dealt mainly with material chemistry considerations for next generation battery electrodes, their response to lithiation and relation to performance. One additional factor that needs to be considered while designing new electrodes is the architecture or arrangement of the active material. The majority of currently available commercial Li ion battery electrodes are formed as thin films on the order of hundreds of microns thick. These films often consist of an active-material powder, polymer-based binders and additives aimed at increasing electric conductivity of the electrode. These additives have a negative effect on the gravimetric energy density, and as such are undesirable, although necessary in current cells. The geometric considerations of the electrode design are important in the light of inherent limitations of the charge transport characteristics of the electrode, and both concentration and activation polarizations. For instance, in $LiFePO_4$ and graphite, the Li ion conductivities are of an order of 10^{-10} cm^2s^{-1}, compared to 10^{-6} cm^2s^{-1} in commonly used electrolytes [21, 159]. Li ions, from the surface of the active material diffuse inwards, filling the vacancies in active materials microstructure, and creating bottlenecks that impede additional ion transport. The structure of the electrodes, their thickness and the length of diffusion pathways, obstruct ionic mobility and limit the batteries to slower rates than could otherwise be possible.

View Article Online
DOI: 10.1039/C4TA00534A

For these reasons, 3-dimensional, porous electrode architectures have attracted a lot of attention, particularly because battery size and mass are expected to be reduced in next generation power systems, without a reduction in energy density in principle. One primary driver for power source improvement and also miniaturization is Moore's Law, which empirically links the increase in the density of transistor elements on a microchip (or the reduction in the feature size for these transistors) with computational power or operations per second, which has incessantly increased since its inception. The performance of portable electronics, batteries, unfortunately has an annual improvement 'curve' characterized by just a 10% increase in energy density.

One analogy between electronic computation speed and improved energy storage and supply materials in battery power sources is the mobility of the charge carriers: electrons and holes for electronics; electrons and ion for batteries. The classical diffusion relation $L^2 \propto D\tau$ shows that a reduction in length scale (L) is beneficial when considering diffusion lengths of Li (or other cations) and the associated diffusion constant (D) into (at least) the pristine active material during discharge (rate dependent). However, battery chemistries during discharge are complex, even for very well understood bulk analog of useful or promising materials; performance improvements can be significant, however, when many factors are taken into account. Inherent transport kinetics unique to certain crystal structures are often predefined and affected by the crystal structure, orientation and chemical potential; size reduction does not automatically improve performance or rate capability. Shorter transport distances (faster times to cation insertion) and higher surface-to-volume ratios that improve redox accessibility and time for ion and electron transport can be achieved when the discharge chemistry and phase formation are well understood. By providing pathways for lithium insertion, phase formation, shorter diffusion lengths in 3D can alleviate rate

View Article Online
DOI: 10.1039/C4TA00534A

limitations or improve cyclability for 'gentler' depths of discharge in many systems. Once at the interface of an active particle, Li ions enter from the outside inward, filling the atomic-scale vacancies in the active material's exterior microstructure and therefore creating diffusion bottlenecks that impede additional ion transport. Acting in concert, the dense nature of electrode composites, electrode thicknesses of ~100s mm, and micrometer-scale diffusion path lengths in active electrode particles obstruct ion mobility and limit lithium-ion batteries to slower discharging and recharging rates than are otherwise possible. These elements also add significant 'dead weight' to all current commercial batteries and would make it extremely difficult to assemble as an ordered smooth layered battery. This design, as will be discussed further on, also allows faster charging and discharging rates, and the possibility of strongly asymmetric charge/discharge cycles optimizing power delivery and shortening charging times. Such changes may first take place in the use of small devices, where the total amount of energy stored is small. Only 360 W is required to charge a 1Wh cell phone battery in 10 s (at a 360 C charging rate, where the C-rate is the inverse of time in hours required to fully charge or discharge an electrode or battery). Even at the highest charge rate tested thus far for these materials (50 C), corresponding to a time of 72 s (as opposed to 3.5 hrs based on the mass of active material in bulk form) to fully discharge the capacity, the material achieves about 80% of its theoretical capacity.

Porous electrodes offer numerous important benefits that are listed below [160]:

- Pores provide good access for the low surface-tension electrolyte to the electrode surface ordinarily taken up with polymer binders and carbon additives that are no longer required.

View Article Online
DOI: 10.1039/C4TA00534A

- Large surface area of the porous electrode facilitates charge transfer across the electrode/electrolyte interface, reducing the impact of the activation polarization.
- Ionic diffusion path-lengths are reduced due to lower wall thickness less than the limiting solid state diffusion length of lithium for discharging and lower overpotential charging.
- The active material is used more efficiently due to better electrolyte penetration and reduced wall thickness.
- Continuous electron pathways are provided from the active material to the external load.
- The volumetric energy density is comparable with packed particle electrodes
- In some cases no binders or conductive additives are required, reducing dead weight (better gravimetric energy density).
- Void spaces separating particles can accommodate volumetric changes of active material.
- Porous composites can incorporate a secondary conductive phase to improve high rate performance of active phases with low intrinsic conductivity.

Depending on the electrode preparation method, porous electrodes can be divided into those that are hard-templated or soft-templated. The size of the pores allows categorization of the porous electrodes as follows: microporous (pore size <2 nm), mesoporous (pore size 2-50 nm) and macroporous (pore size >50 nm).

Soft templating usually involves surfactants as structure directing agents. The pore architecture can be controlled by the choice of surfactants, solvents and synthesis conditions. Evaporation induced self-assembly (EISA) is particularly useful for formation of thin films with

View Article Online
DOI: 10.1039/C4TA00534A

precisely controlled porosity [161]. It can be however difficult to obtain high crystallinity of the walls of the solid, if the temperature of the crystallization of the inorganic phase is higher than the temperature at which the surfactant block copolymer is removed. In this situation, hard templating approaches are much more successful. Templates such as aluminium anodic oxide (AAO) membranes, preformed porous solids, and assemblies of colloidal particles are used.

6.1 AAO templated nanomaterials

Figure 11 presents a schematic of formation of porous material using AAO template, with isolated pores. In this case, solid products form inside the template, replicating the shape of the void space. Usually, structures such as 1D nanotubes and nanowires are formed. AAO templates are commonly used, due to ease of the preparation of the template, as well as uniform pore size [162]. AAO membranes can also be used in conjunction with soft templating materials to prepare solid structures with hierarchical porosity [163]. A variety of inorganic electrode materials can be prepared using this method, including metals, metal oxides and various composites.

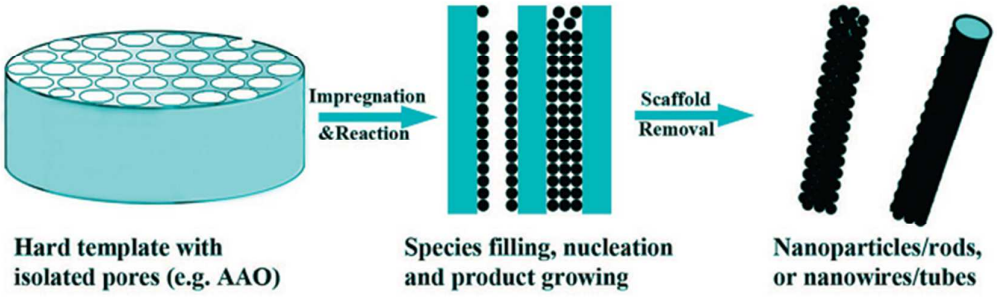

Figure 11 AAO templating mechanism. Reproduced from [164] the American Chemical Society.

View Article Online
DOI: 10.1039/C4TA00534A

6.2 Nanocasting of nanoscale battery materials

Nanocasting is a name given to the transformation of a porous solid into hollow replicas. In the nanocasting process, porous solids are infiltrated with the precursor of target electrode material (see Figure 122). After thermal treatment, the template is removed. The product is an inverted replica structure of the original hard template. The molds with bicontinuous pore structures produce mesoporous replicas, whereas templates with cylindrical mesopores in hexagonal arrangement produce nanowire arrays, which are interconnected only if the template contains secondary pores between the main cylindrical pores.

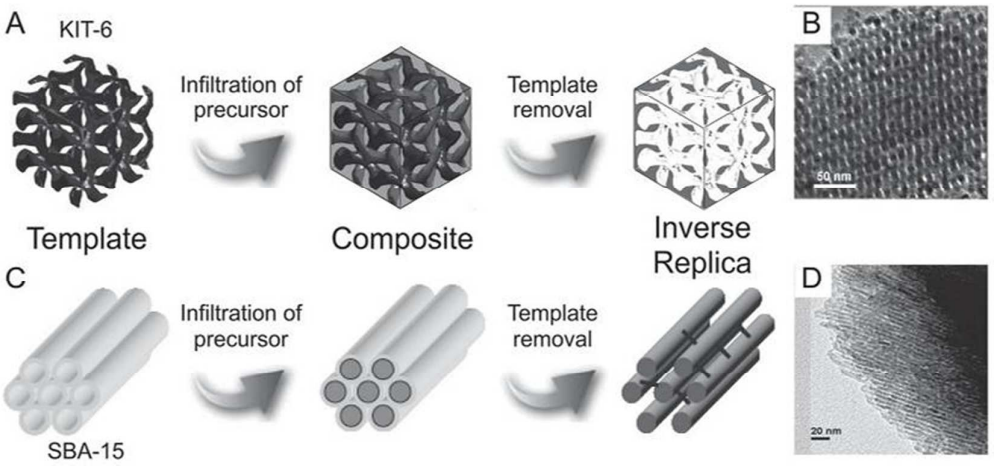

Figure 12. Nanocasting of mesoporous electrode materials. (a) Nanocasting process in mesoporous silica. (b) TEM image of mesoporous TiO_2. Reproduced from [165] with permission from the German Chemical Society. (c) Nanocasting process in mesoporous silica SBA-15 Reproduced from [84] with permission from the the American Chemical Society. (d) TEM image of mesoporous Si-C nanowire formed from SBA-15 template.

The most commonly used hard templates are mesoporous silica materials. To remove these template materials, simple wet etches can be carried out, either through extraction with HF, hot NaOH or KOH solutions. Mesoporous electrodes with numerous compositions have been synthesized by hard templating, including MnO_2 [166, 167], Cr_2O_3 [168], Co_3O_4 [169], SnO_2 [170] NiO [171]. In particular, SnO_2, nanocasting allows the formation of

View Article Online
DOI: 10.1039/C4TA00534A

mesoporous solids with a higher degree of crystallinity, and more order compared to soft templating, due to protection from excessive grain growth by sintering present in soft-templated materials [160].

6.3 Colloidal crystal templating

Colloidal crystal templating allows for the formation of porous electrodes with an excellent degree of control over the pore size and the template solid structure. Facile templating methods are compatible with a variety of precursors and allow the formation of inverted opals (IO) of many materials. The general procedure for IO preparation is demonstrated in Figure 13, where a hard template is infiltrated by an appropriate precursor, and then removed either chemically or thermally.

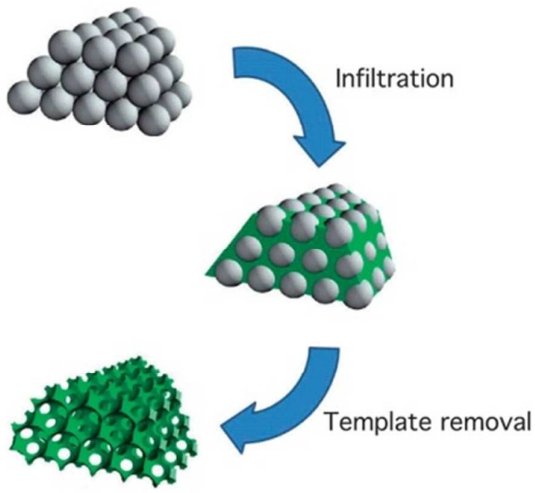

Figure 13. Schematic diagram detailing preparation of inverted opal electrode. Reproduced from [172] with permission from the Royal Society of Chemistry. Through various mechanisms, the arrangement of spheres dictates the periodic porosity of the resulting inverted opal structure.

View Article Online
DOI: 10.1039/C4TA00534A

The template preparation mechanism generally involves self-assembly of template spheres (usually a hard polymer like polystyrene or poly(methyl methacrylate), [173] or silica on the surface of the substrate. This makes it possible to form inverted opal structures of a variety of metals and metal oxides [160, 172, 174, 175] and metal fluorides [176]. Typically, inverted opals have wall thicknesses in the range of 10s to 100s of nanometres, and have been prepared and characterized in multiple compositions, for Li ion anodes, cathodes and solid state electrolyte materials.

IOs generally exhibit higher power densities than bulk materials, due to excellent electrolyte penetration. Although they may not the best choice for electrodes composed of materials which undergo large volumetric expansion upon lithiation (e.g. alloying materials), using a bicontinuous approach allows for formation of IO electrodes from alloying materials as well. Excellent control over the morphology of the IOs and an extensive range of compositions make IO structures very exciting in other areas of research, ranging from catalysis[177], gas sensing, to optics and filtration.

The following section will detail the various implementations of IO structures as active materials for LIB anode and cathodes.

7. Inverted Opal structures for Lithium ion battery applications

7.1 Inverted opal cathode

Vanadium oxide was the first material to be electrochemically characterized as a cathode material in an inverted opal arrangement [178]. In this study, colloidal crystals consisting of polystyrene spheres was deposited on an ITO glass current collector and infiltrated with a

View Article Online
DOI: 10.1039/C4TA00534A

diluted vanadyl alkoxide precursor. Subsequently, the precursor was transformed into solid V_2O_5 gel network. (see Figure 14).

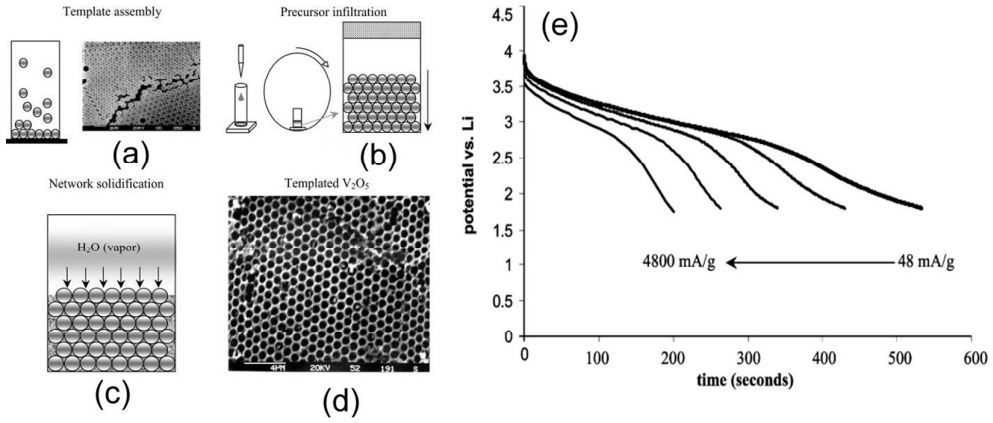

Figure 14. (a-d) Schematic diagram detailing formation of V_2O_5 IO cathodes. (e) Rate performance of the V_2O_5 IO cathodes. Reproduced from [178] with permission from the Royal Society of Chemistry.

Chemical removal of PS sphere template results in the formation of inverted opal structures of V_2O_5 amibgel. At low discharge rates, the ambigel electrodes exhibit reversible behaviour without significant loss of capacity. This study also demonstrated excellent rate performance of IO based electrodes, indicating that the hierarchical structure might reduce polarization via improved mass transport. Electrochromic properties of an IO prepared from V_2O_5 have been also demonstrated [179] demonstrating improvements such as faster switching speed and better coloration contrast, when compared to bulk films.

In a different study, $LiCoO_2$ was formed in an IO structure through a nanocasting route. Mixed precursors of Li and Co salts precipitate as oxalates within colloidal crystal template voids [180]. At precursor ration of 1:1, it is possible to form $LiCoO_2$, however, it is difficult to preserve the IO structure due to the high temperatures required for the formation of the $LiCoO_2$ phase. None of the $LiCoO_2$ powders formed, even with addition of PEG as

View Article Online
DOI: 10.1039/C4TA00534A

chelating agent, preserve the IO structure. However, the high interconnectivity and large porosity of the sample allows sustaining high rate cycling. At 700 mAg^{-1}, the mesoporous structure of $LiCoO_2$ is able to sustain a capacity of 40 mAg^{-1}, while the corresponding bulk film fails to charge due to high polarization.

Another binary oxide formed as an IO structure ($LiNiO_2$) was prepared through a salt precipitate procedure [181]. Stoichiometric $LiNiO_2$ has a layered structure in which Li^+ ions occupy octahedral sites in alternate layers of cubic close packed (ccp) oxide ions. At high temperatures, $LiNiO_2$ readily decomposes to $Li_{1-x}Ni_{1+x}O_2$ due to vapour pressure differences between Li salts and formation of Ni^{2+}. Adding excess Li salt and introducing higher oxygen gas partial pressure to suppress reduction of Ni atoms, allows formation of IO structures.

$LiMn_2O_4$ spinels were fabricated using precursors that solidify before destruction of colloidal crystal template during annealing [182]. Gradually increasing the temperature, however, during template removal, allowed for transformation of amorphous Li-rich sites within the electrode to spinel phase with Li ions in tetrahedral and octahedral sites. $LiMn_2O_4$ showed remarkable capacity retention, with no more than 7% capacity loss after 10000 full cycles at 9 C (full discharge in ~7 minutes) (see Figure 15) , compared to more than 80% reduction in the charge capacity for bulk $LiMn_2O_4$.

View Article Online
DOI: 10.1039/C4TA00534A

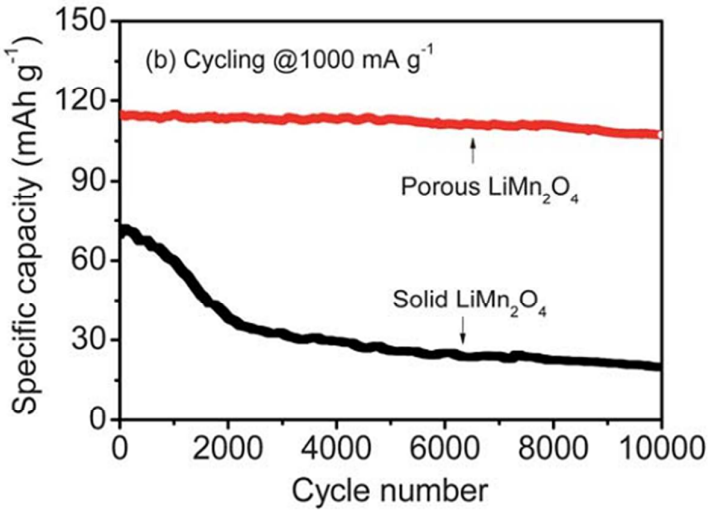

Figure 15. Cycling behaviour of solid and porous $LiMn_2O_4$ electrodes. Reproduced from [182] with permission from the Royal Society Chemistry.

The excellent electrochemical performance of IO electrodes can be ascribed to high crystallinity, ensuring stability during cycling; high degree of porosity, shortening diffusion lengths and a reduction of polarization.

Lithium iron (II) phosphate is an alternative cathode material that has been extensively researched since the original paper on the material application in battery electrodes in 1997 [183]. Iron represented a cheaper alternative to expensive cobalt and nickel materials. However it suffers from low ionic and electronic conductivity, making high power applications difficult to realize. The IO structure should improve the ionic conductivity by providing nanoscopic walls with shortened diffusion lengths and opened pore networks that facilitate electrolyte penetration. Lu et al. [184] prepared $LiFePO_4$ IOs by mixing Li, P and Fe precursors in stoichiometric ratio. Subsequent calcination under nitrogen resulted in the formation of IOs with residual carbon interspersed in the $LiFePO_4$. The carbon content

View Article Online
DOI: 10.1039/C4TA00534A

contributed to the conductivity of the IO and allowed for high charge rates, resulting in an initial capacity of 100 $mAhg^{-1}$ at 5.9 C.

Recently, Doherty et al. described the preparation of $LiFePO_4$ IOs based on PMMA colloidal templates, with sphere sizes varying from 100-270 nm [185]. The templates were not filled completely, which improved the electrolyte penetration and ionic and electronic charge transfer. Sintering at 800 °C improved charge transfer resistance in the electrodes and allowed for charge rates of 10 C with capacity retention close to 100 $mAhg^{-1}$ after 50 cycles. Template sphere size was also shown to have an influence on the electrochemical performance of the IO electrodes, as larger spheres created a continuous macropore network, ensuring facile flow of the electrolyte to all of the parts of the electrode. Residual amorphous carbon present after calcination in N_2 also enhanced electronic conductivity of the olivine material, although a balance is necessary, as high weight percentage of C may create a Li diffusion barrier and hinder high rate performance.

8. Inverted opal anodes

8.1 Carbonaceous inverted opal anodes

Graphitic carbon is currently used in commercial LIB as an anode electrode. It offers excellent stability, and relatively long cycle life (1000s of cycles). However, its performance at high discharge rates is hindered by low Li ionic conductivity in carbon. IO structure offers a possibility to improve the performance of carbon based electrodes, through facilitating easier electrolyte penetration and shortening Li ion diffusion lengths in active material matrix. The first C-based IOs were prepared in 1998 by Zakhidow et al [186], via a vapour deposition technique, forming diamond, glassy carbon and graphite inverted opals were

View Article Online
DOI: 10.1039/C4TA00534A

published. Solution based processes for carbon IO formation were then reported, using sucrose [186] and phenyllic resin [187] as carbon precursors. In 2005, two separate articles investigating the electrochemical performance of carbon based inverted opal electrodes. In one approach [188] PMMA templates were infiltrated with resorcinol-formaldehyde (RF) sol gel precursor. This allowed the formation of IO monoliths with mesoporous walls and a surface area of 326 m^2g^{-1}. Large surface area is associated with randomly distributed micropores between the graphene nanosheets in hard carbon solid walls.

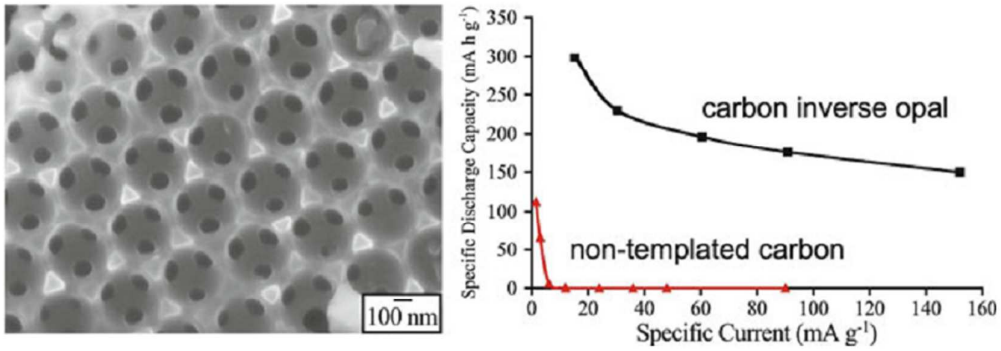

Figure 16. SEM image of carbon inverted opals. Carbon inverted opals experience much less polarization than bulk carbon of same composition. Adapted from [188] with permission from Wiley-VCH.

The monoliths were found to be electronically and ionically conductive. Good conductivity, excellent electrolyte penetration related to the porosity of the IO and shortened diffusion path lengths allowed carbon IOs to experience much less polarization at current rates as high as C/2. (Figure 16).

In another study, carbon IOs were prepared by CVD of benzene using silica IOs as templates [189]. The resultant 10-20 nm coating of graphite on silica was electronically and ionically conductive and was suited as an anode active material. This material exhibited

View Article Online
DOI: 10.1039/C4TA00534A

specific capacities as high as 260 $mAhg^{-1}$ at current rates of 1000 mAg^{-1} (~2.7C), with good cycling stability (90 % capacity retention over 60 cycles).

More recently, particulate inverse opal structures with mesoporous walls were prepare via solution casting of PS spheres with phloroglucinol and formaldehyde mixture containing F127 block copolymer [190]. Incorporating soft templating methods into the IO formation procedure resulted in increased surface area (from 109 m^2g^{-1} to 466 m^2g^{-1}). A large irreversible capacity was attributed to formation of SEI layer on the electrode, and inherent properties of hard carbon. The mesoporous carbon was however capable of sustaining charge rates as high as 300 mAg^{-1} with reversible capacity of over 300 $mAhg^{-1}$.

An interesting means of increases the capacity of carbon based IOs is to introduce a secondary active material, usually in a form of nanoparticles embedded in the conductive matrix of carbon IO. Materials such as SnO_2 [90, 189], Si [191] or TiO_2 [192] have been incorporated in the carbon based inverted opals, with significant influence on the electrochemical performance[193]. One of the most recent studies demonstrated an IO electrode concept with SnO_2 NPs entrapped in macroporous carbon IO prepared by infiltration of PMMA colloids by tannic acid Sn^{4+} complexes [90]. Optimization of infiltration and calcination parameters resulted in nanometre scale walls and improvement in the rate performance of the electrodes. They were able to sustain current rates in the range of 1-10 Ag^{-1} (~3-30 C) without any significant capacity loss. High porosity (including hierarchical length scale of multiple porosities) in the electrode resulted in low volumetric energy density of prepared electrodes, confirming the need for further improvements in the electrode design. With respect to inverse opals, three-dimensionally interconnected macropores facilitate the rapid flux of liquid electrolyte solutions, such that 100 m^2 g^{-1} of electrode interfaces are

View Article Online
DOI: 10.1039/C4TA00534A

simultaneously accessible to Lithium or other mobile cationic charges. This degree of macropore interconnectivity is intentionally tailored into PhCs from self-assembled close-packed templates. For example, the ionic conductivity of a 1 M $LiPF_6$ liquid electrolyte solution is only impeded by a factor of two when ion transport occurs through the interconnected macropores of monolithic carbon inverse opals (electrode thicknesses: 300 μm–3 mm).

8.2 Three-Dimensionally structured alloying anodes

The first reports of alloying electrodes in IO form appeared in 2004 [194]. PMMA colloidal crystal templates were infiltrated with $SnCl_2$ dissolved in DI water and 30 wt% H_2O_2. IOs of SnO_2 were formed after thermal removal of PMMA template. The morphology of the walls of IOs was influenced by the calcination temperature, becoming more granular and interrupted by grain boundaries with the increase in the calcination temperature[175]. Galvanostatic cycling of the IOs resulted in significant morphological changes in the electrodes. The wall thickness increased significantly on the alloying of SnO_2 with Li, with nodules appearing on the previously smooth structure (see Figure 17).

View Article Online
DOI: 10.1039/C4TA00534A

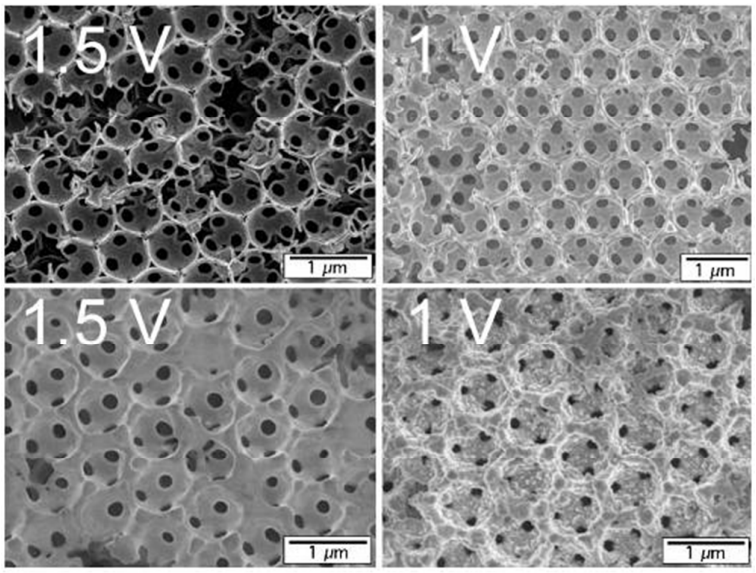

Figure 17. SEM images showing morphologies of SnO_2 IOs at different stages of charging. Reproduced from [194] with permission from the Royal Society of Chemistry.

Repeated cycling caused increase of the wall thickness, and finally loss of the IO morphology. The authors concluded that the large volumetric expansion of the IO SnO_2 electrodes made them impractical for applications in LIBs. Additionally, the granular structure of the SnO_2 walls caused very high polarization, caused by high resistance of the granular walls of the IO. Different approaches were used to alleviate the drawbacks caused by the properties of SnO_2. Using a carbon-SnO_2 composite was one of the strategies employed [189, 195]. Stable capacity of 300 $mAhg^{-1}$ could be delivered by carbon SnO_2 composite at 100 mAg^{-1}. The improved cyclability was attributed to the confinement effect provided by the mesoporous carbon framework, which served as a structural buffer for volume variation of Sn nanoparticles during repeated cycling. Stability of the SEI layer also contributed to the good cyclability of the IOs.

View Article Online
DOI: 10.1039/C4TA00534A

In another approach, Ni support was used to improve the stability of the SnO_2 IO based electrode [196]. In this study, a colloidal crystal template was infiltrated using electroplating. A mixture of $SnCl_2$ and $NiCl_2$ was deposited from an aqueous solution through electroplating, and tested electrochemically. Repeated cycling caused delamination of the IO electrode from the current collector, possibly due to epitaxial mismatch of the Ni-Sn alloy and the Cu current collector. During cycling, the electrode underwent rapid morphological changes and as a result, capacity retention was poor. After 100 cycles, the reversible capacity sustained by the electrode was only about 95 $mAhg^{-1}$.

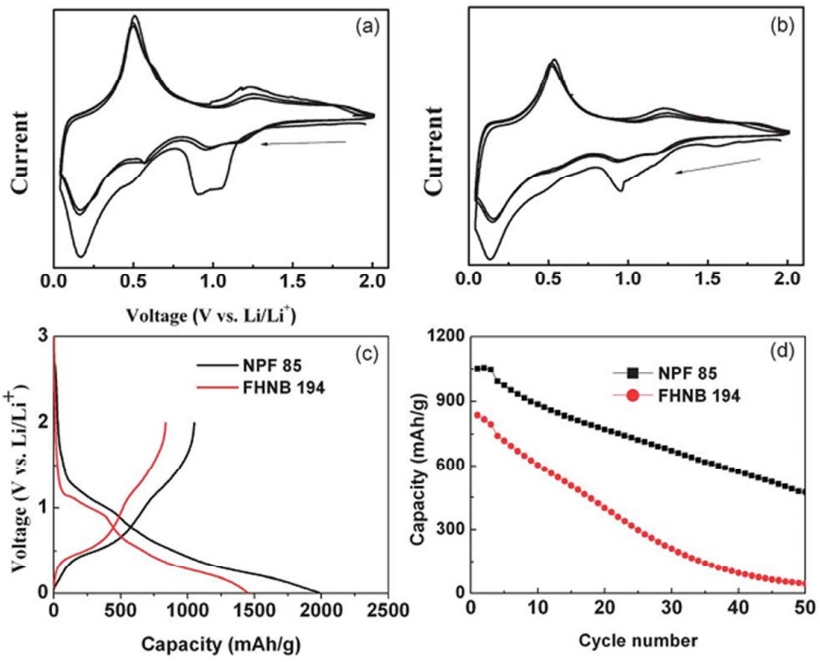

Figure 18. (a) CV for hollow FTO. (b) CV for porous FTO. (c) Initial charge and discharge curves for porous FTO. (d) Cyclic performance for porous FTO. Reproduced from [197] with permission from the Royal Society of Chemistry.

Recently, [197], fluorinated tin oxide (FTO) and antimonated tin oxide (ATO) IOs showed significant improvements in electrochemical performance compared to pure SnO_2 IOs, in

View Article Online
DOI: 10.1039/C4TA00534A

both capacity and cycling stability (see Figure 18). The improved performance of the FTO and ATO electrodes was attributed to improved integrity of the nanoporous structure, allowing for better tolerance of large volume changes caused by repeated cycling of the electrode. Good electrochemical performance of highly conductive transparent oxides may enable their applications in solar cells, electrochromic devices or sensor applications.

Si is another material that has been investigated electrochemically and structurally in IO architecture. Esmanski et al. [198] prepared a variety of Si based IO films: amorphous hydrogenated Si IOs (prepared through CVD), nanocrystalline Si-IOs, carbon coated nanocrystalline Si-IOs and carbon IOs with amorphous Si coating. Amorphous hydrogenated Si IOs demonstrated good initial discharge capacity (2500 $mAhg^{-1}$). The cycling stability of the IO electrodes was also satisfactory, with over 70% of discharge capacity retained after 145 cycles. Sphere size was also shown to have an influence on the performance of the IOs, as the electrodes prepared from templates with lower diameter spheres performed poorly, due to blockage of the pore openings by swelling electrode material. The rate performance of the IO was limited by the amorphous structure of the IO walls. In order to increase conductivity, amorphous IOs were annealed at 800 °C in an inert atmosphere resulting in the formation of nanocrystalline Si-IO. The crystalline structure of the IO walls resulted in improved Li mobility in the electrode material, and better rate performance. Capacity retention however was extremely poor, reaching negligible values by the 15^{th} cycle at best. Similar electrochemical behaviour was observed for carbon coated nanocrystalline Si IOs.

In the same study, a different approach was also presented. Carbon IOs were coated with thin layer of amorphous Si via CVD. The initial capacity of the IOs was around 2000 $mAhg^{-1}$, with the first cycle coulombic efficiency reaching around 80%, increasing to 98-99%

View Article Online
DOI: 10.1039/C4TA00534A

after 5th cycle. The rate performance of the IO was poor, compared to amorphous Si samples, with the capacities reaching negligible levels at 10C rates. The carbon support allowed for better mechanical and structural stability of the IOs, resulting in good capacity retentions of over 80% after 145 cycles. Esmanski's findings agreed well with results published by Kim et al [92], who prepared 3D porous Si particles through deposition of sol-gel mixtures of Si and silica particles and subsequent HF etching. The 3D particles demonstrated excellent capacity retention and rate capability, delivering 2668 $mAhg^{-1}$ after 100 cycles at 1C rate.

In a more recent study, nanoscale Ni metal scaffold supported bicontinuous 3D IO based batteries were prepared by Paul Braun's group[199]. The formation mechanism for these electrodes is shown in Figure 19.

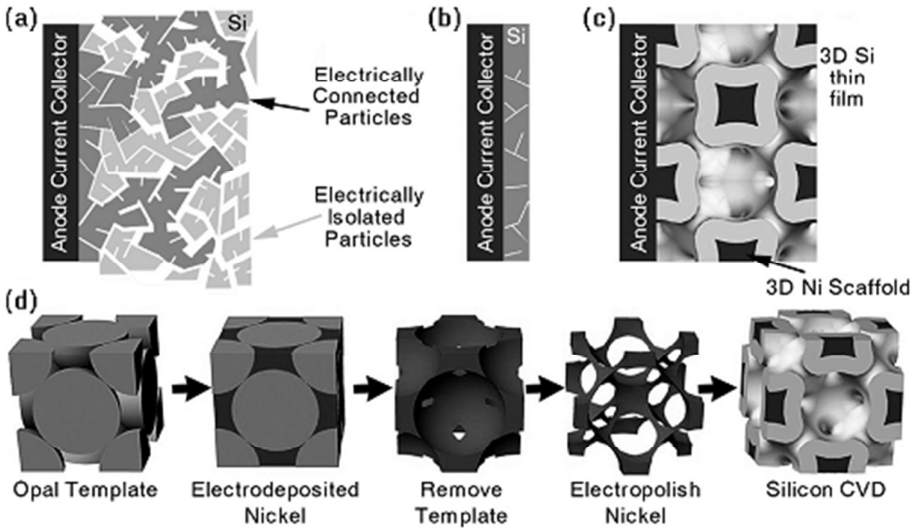

Figure 19. (a) Loss of electrical contact during cycling. (b) Good electrical contact between Si film and Ni substrate. (c) Bicontinuous bulk anode consisting of silicon thin film on 3D porous Ni scaffold. (d) Fabrication procedure for the bicontinuous electrode Reproduced from [200] with permission from Nature Publishing Group.

View Article Online
DOI: 10.1039/C4TA00534A

Initially, nickel was electrodeposited in a PS template. Following thermal template removal, the Ni IO was electropolished and a thin film of Si was deposited on the surface of Ni support through CVD. The self-supported Si anodes showed excellent electrochemical performance, delivering stable capacity of 2660 $mAhg^{-1}$ while conserving over 48% of its slow rate capacity when charged at 9.5 C.

The same bicontinuous approach was also successfully employed in an operational battery [200], where MnO_2 cathodes were prepared by electrodeposition of $MnSO_4$ on electropolished Ni metal current collector. Superior rate performance of the bicontinuous films was attributed mainly to excellent electrolyte penetration, reduced polarization by providing a low resistivity current collector throughout the electrode and shortened diffusion lengths. Such prepared electrodes were able to deliver capacities of over 75 $mAhg^{-1}$ at an exceptionally high rate of 1114 C, which corresponds to full discharge in less than 4 seconds (see Figure 20).

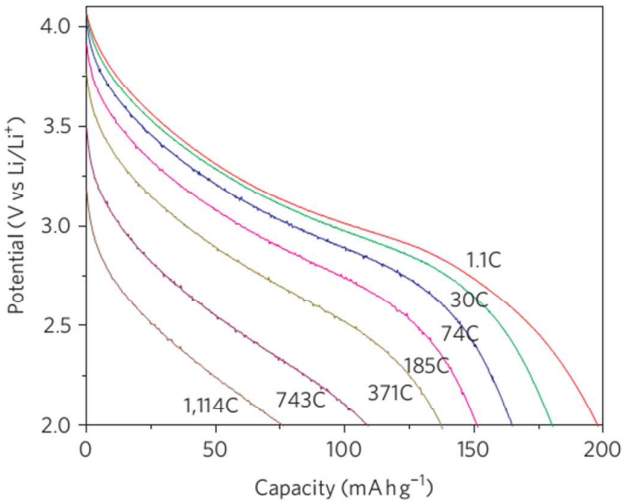

Figure 20. Ultrafast discharge of the lithiated MnO_2 cathode. Reproduced from [200] with permission from Nature Publishing Group.

View Article Online
DOI: 10.1039/C4TA00534A

The most recent report [201] concerning 3D battery architectures, describes a high power microbattery capable of delivering power densities as high as 7.4 mW cm^{-2} μm^{-1} (see Figure 21). In this study, polystyrene spheres were deposited over gold electrodes etched on glass substrate. Subsequently, a nickel metal support was electrodeposited over the gold electrodes to form a stable current collector. A Ni-Sn alloy and MnOOH were then electrodeposited on the current collector, before submersion of the microbattery in $LiNO_3$ and LiOH, to form a lithiated cathode. Such microbattery design allowed the authors to achieve over 2000× the power and twice the energy density observed in the best microbattery designs presented thus far. The energy densities demonstrated of up to 15 μWh cm^{-2} μm^{-1}, and the power densities of up to 7.4 mW cm^{-2} μm^{-1} are comparable with the best supercapacitors. The improvements in power and energy density were attributed to shortened ionic diffusion lengths, and reduced resistivity of the electrode. Successful demonstration of a high power microbattery allows compact integration of a full battery package for microelectronics applications. The versatility of this approach also permits development of different types of electrode chemistry for specific applications.

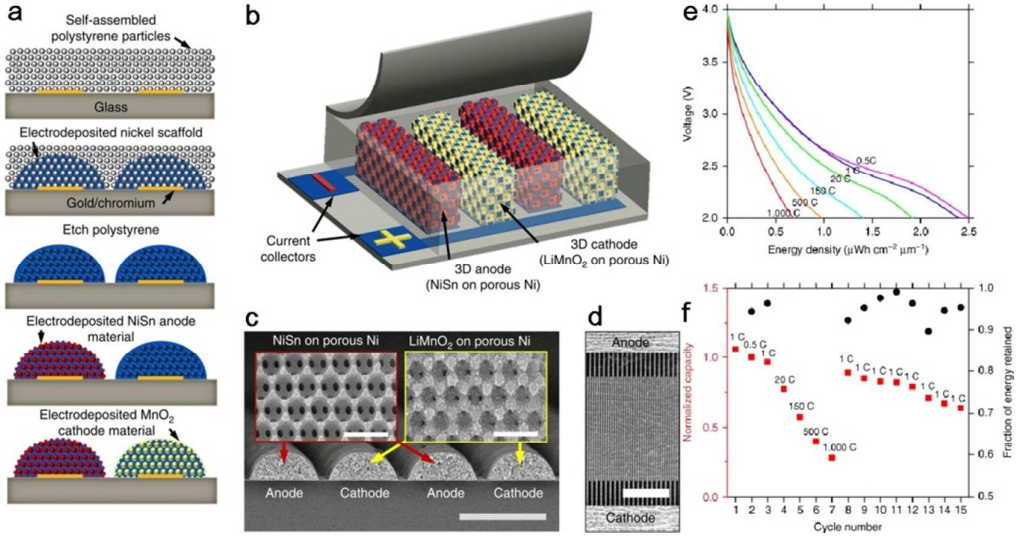

View Article Online
DOI: 10.1039/C4TA00534A

Figure 21. (a) Schematic diagram of microbattery fabrication procedure. (b) Microbattery design. (c) SEM cross-section of the microbattery. (d) Top-down SEM image of the microbattery interdigitated electrodes. (e) Constant current line sweeps at different rates. (f) Rate performance of the microbatteries. Adapted from [201] with permission from Nature Publishing Group.

Table 3 summarizes some of the developments in IO Li-ion battery electrode research.

Composition	Morphology	Initial capacity (C-rate)	Final capacity (# of cycles)	Ref
V_2O_5	IO	-	-	202
$LiNiO_2$	IO	-	-	
SnO_2	IO	-	-	194
C	IO	299 (15.2 mAg^{-1})	-	188
Sn/C	Sn@C IO	348 (15.2 mAg^{-1})	-	
C	Graphitic C IO	326 (C/10)	320 (60)	189
Sn/C	Sn@C	415 (C/10)	375 (60)	
TiO_2/C	TiO_2@C	158 (50 μAcm^{-2})	40 (15)	203
$Li_4Ti_5O_{12}$	IO	152 (6.3μAcm^{-2})	145 (70)	204
$Li_4Ti_5O_{12}$	IO	173 (C/10)	120 (100)	205
$FePO_4$	IO	137 (C/10)	110 (50)	206
$LiMn_2O_4/Li_{1.5}Al_{0.5}Ti_{1.5}(PO_4)_3$	IO composite	64 (-)	-	207
$LiMn_2O_4$	IO	-	-	208
Sn/C	Sn@C	1500 (100 mAg^{-1})	96 (100)	195
Si/C	Si@C	3180 (-)	-	191
$LiFePO_4$	IO	115 (5C)	120 (50)	185
Si	a-Si:h IO	2500 (C/10)	1750 (145)	
	nc-Si IO	3000 (C/10)	0 (15)	198
Si-C	nc-Si-C IO	2400 (C/10)	0 (12)	
	a-Si-C IO	2406 (C/10)	2133 (145)	
Ni/Sn	Ni-Sn Composite	315 (50 mAg^{-1})	~100 (100)	196
$LiMn_2O_4$	IO	-	-	182
MnO_2 @ Ni	Thin film/IO Bicontinuous	74 (1114 C)	-	200
FeF_3	IO	540 (50 mAg^{-1})	190 (30)	176
Si @Ni	Bicontinuous IO	3568 (C/20)	2660 (100)	199
SnO_2/C	SnO_2@C	1659 (0.5 Ag^{-1})	715 (500)	90
TiO_2	IO	442 (25 mAg^{-1})	117 (200)	209
C	IO	359 (-)	315 (20)	190

Table 3. Summary of the performance of various types of IO based electrodes.

View Article Online
DOI: 10.1039/C4TA00534A

9. Pseudocapacitors that offer good power and energy densities

Capacitive charge storage has some particular advantages compared to non-faradaic intercalation batteries. Supercapacitors can be charged within seconds, cycled hundreds of thousands of times, are stable and ideal for delivering high power, which for some uses is preferably to a higher energy density.[210] Several options exists for charge storage at the electrode-electrolyte interface, which are sensitively dependent on structure and composition, chemical potential redox potential and many other factors. In secondary or rechargeable batteries, cations intercalate into interlayer gaps (van der Waals gaps) of layered or tunnel materials [211] or form alloys with phases of other materials. The specific type of materials that permit intercalation however, can offer in some conditions, faradaic and non-faradaic processes, thereby adding energy and power density benefits of both systems.

Cations that can electrochemically adsorb onto the surface of a material through charge-transfer processes facilitating non-intercalation based charge storage, similar to electrochemical double layer capacitors to some extent. This can in some cases remove the limitation of long diffusion times for ions through the van der Waals gaps, and is energetically easier. Such pseudocapacitance when this form of insertion is capacitive, i.e. the electrochemical intercalation processes stem from cations that are faradaically stored and changes in materials structure do not occur.[212] While there are many text-books that deal with the fundamentals of capacitive and intercalation charge storage mechanisms, there are some salient features that are important for materials that ordinarily store charge through intercalation, but exhibit surface charge storage when polarised at higher rates.

View Article Online
DOI: 10.1039/C4TA00534A

Increasing the rate of a cyclic voltammagram for structured or porous energy storage materials has a large influence on the course of the electrochemical reaction many cations. One characteristic is that the current peaks associated with many processes such as SEI formation, reduction, oxidation, alloying or intercalation, are often convoluted within the total cumulative charge and the curve resembles that of an asymmetric supercapacitor to some degree. The current response is however much larger than for the slow rate scan, suggesting that there is additional charge storage mechanism operating at large potentials. The total stored charge, for any electrochemical energy storage process can be separated into three components: The faradaic contribution from the Li^+ ion insertion processes, the faradaic contribution from the charge transfer process with the surface atoms, referred to as pseudocapacitance and the non-faradaic contribution from the double layer effect [213]. When the porosity of the electrode increases, both types of capacitive contributions (pseudocapacitance and double layer charging) can be significant. The capacitive effects can be characterized by analysing data from cyclic voltammetry experiments carried out at different scan rates, according to [214]:

$$i = av^b \quad (1)$$

where the measured current i obeys a power law relationship with the sweep rate v. Both a and b are adjustable parameters, with b value, determined from the slope of $\log(i)$ vs. $\log(v)$. There are two well-defined conditions, $b = 0.5$ and $b = 1$. For $b = 0.5$ the current is proportional to the square root of the scan rate, according to the equation:

$$i = nFAC^*D^{\frac{1}{2}}v^{\frac{1}{2}}\left(\frac{\alpha nF}{RT}\right)^{\frac{1}{2}}\pi^{\frac{1}{2}}\chi(bt) \quad (2)$$

View Article Online
DOI: 10.1039/C4TA00534A

where C^* is the surface concentration of the electrode material, α is the transport coefficient, *D* is the chemical diffusion coefficient, n is the number of electrons involved in the electrode reaction, *A* is the surface area, *R* is the molar gas constant, *F* is the Faraday constant, *T* is the temperature, and $\chi(bt)$ represents the normalized current for a completely irreversible system, as indicated by cyclic voltammetry.

The other defined condition is when $b = 1$, which is representative of capacitive response, as the capacitive current is proportional to the scan rate, according to:

$$i = vC_dA \quad (3)$$

To obtain the *b*-value for a given material system, current values from cyclic voltammagrams carried out at different scan rates are recorded at specified potential values. Then, the slope of the plot of the $\log(i)$ vs $\log(v)$ is the *b*-value at that potential.

As a pertinent example of many in the literature, Brezesinski et al. [215] recently showed that controlling the morphology of mesoscale porous materials such as films of iso-oriented α-MoO_3 can facilitate a change from non-faradic process to a mixture that helps increase the overall energy density of capacitor-based storage devices, using pseudocapacitive effects controlled by reaction kinetics. These properties were unique to their mesoporous crystalline materials and were superior to those of either mesoporous amorphous material or non-porous crystalline MoO_3 (See Figure 22). The iso-oriented layered crystalline domains enabled Li-ions to be inserted into the van der Waals gaps of the α-MoO_3 and importantly, occurs on the same timescale as redox pseudocapacitance.

View Article Online
DOI: 10.1039/C4TA00534A

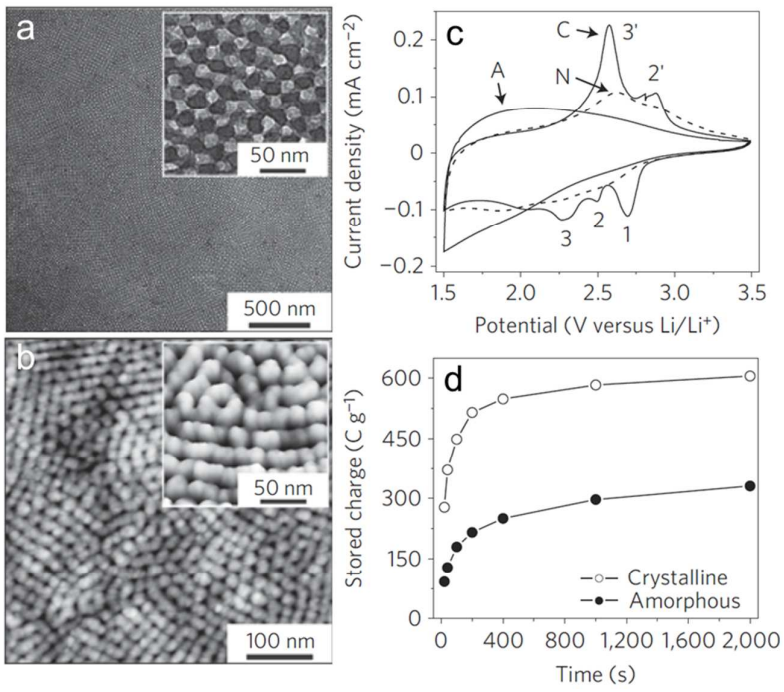

Figure 22 (a) Morphology of mesoporous α-MoO_3 with highly oriented crystalline walls. Low-magnification bright-field TEM micrograph. Inset: A higher magnification micrograph. (b) AFM image of the top surface. Inset: A tilted AFM image with height variations in the 1–5 nm range. (c) Cyclic voltammograms for mesoporous amorphous and crystalline films of MoO_3 systems at a sweep rate of 1 mV s^{-1}. (c) Kinetic behaviour of the various mesoporous films. The total amount of charge storage (gravimetrically normalized) as a function of charging time for each film. Adapted from [215] with permission from Nature Publishing Group

As electrochemically active materials approach nanoscale dimensions, pseudocapacitive effects become increasingly important.[216] In a recent report, Dunn et al. established the dependence of pseudocapacitance on the particle size of anatase TiO_2 nanocrystals.[213] The results showed that for particles smaller than 10 nm in diameter, more than half of the total stored charge is capacitive. As anatase TiO_2 has no van der Waals gap, all of its capacitance is believed to be redox pseudocapacitance. Layered crystal structure materials have also been shown to exhibit such phenomena. TiO_2(B), TiS_2 and $H_2Ti_3O_7$ are able take up LiC through pseudocapacitive processes [217, 218]. In cases where redox

View Article Online
DOI: 10.1039/C4TA00534A

pseudocapacitance contributes to the overall energy density, its contribution can be established by cyclic voltammetry. By varying voltage sweep rates, a transition from faradaic to non-faradaic processes can be assessed in many forms of high surface area materials.

The performance of most advanced IO based LIBs can be compared to a different type of device that is able to simultaneously deliver high power and high energy densities are pseudocapacitors, which store energy electrochemically between two electrode plates. As the energy storage employs fast and reversible redox reactions between electrodes and the electroactive species, most pseudocapacitors use metal oxides with high number of valence states. They are however difficult to mass produce, and suffer from energy density loss at high scan rates. A recent study by Li et al. [219] demonstrated $Ni(OH)_2$ nanospheres with excellent electrochemical performance (see Figure 23), related to high purity of the surface of the nanospheres, large surface area and the amorphous phase of the nanospheres.

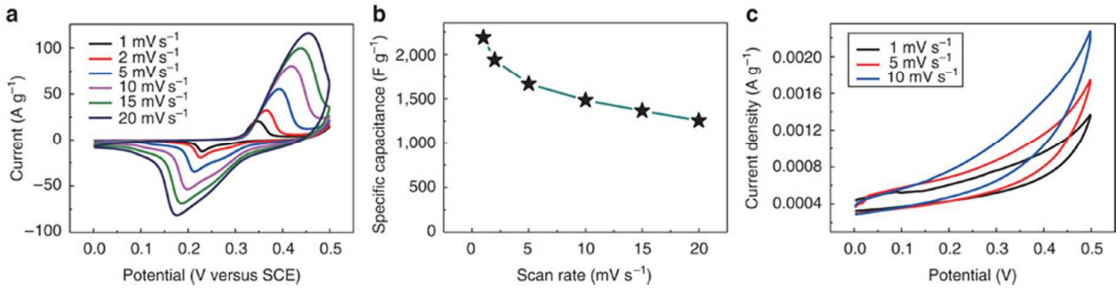

Figure 23 (a) CV curves of the amorphous $Ni(OH)_2$ nanospheres at various scan rates in 1□M KOH. (b) Specific capacitance of the amorphous $Ni(OH)_2$ nanospheres as a function of the scan rates based on the CV curves. (c) CV curves of the blank electrode at various scan rates in 1□M KOH. Reproduced from [219] with permission from Nature Publishing Group.

In a different study, graphene based supercapacitors were prepared by microfabricating electrodes and subsequent deposition of reduced graphene oxide, on both flexible and robust substrates [219]. The energy density of such structures is comparable with

View Article Online
DOI: 10.1039/C4TA00534A

the energy density of LIBs, while their power densities are higher than power densities of capacitors based on metal oxides. Altering carbon-based electrodes and structuring them with ordered 3D porosity was also demonstrated recently by Huang et al. [90]. By creating SnO_2 nanoparticles inside an inverted opal carbon matrix (Figure 24), they demonstrated improved anode kinetics in a Li-ion battery cell. The electrodes exhibit simultaneously enhanced ion and electron transport kinetics as well as geometrically constrained active nanoparticles delivering up to 94.17% of theoretical capacity over 1000 discharge/charge cycles at a current density of 2.0 A g^{-1}, and exhibits good rate capability in the high current density range of 1.0–10.0 A g^{-1}. Creating hybrid materials with two or more active materials offers some potential advantages depending whether energy density and/or cycle life are important.

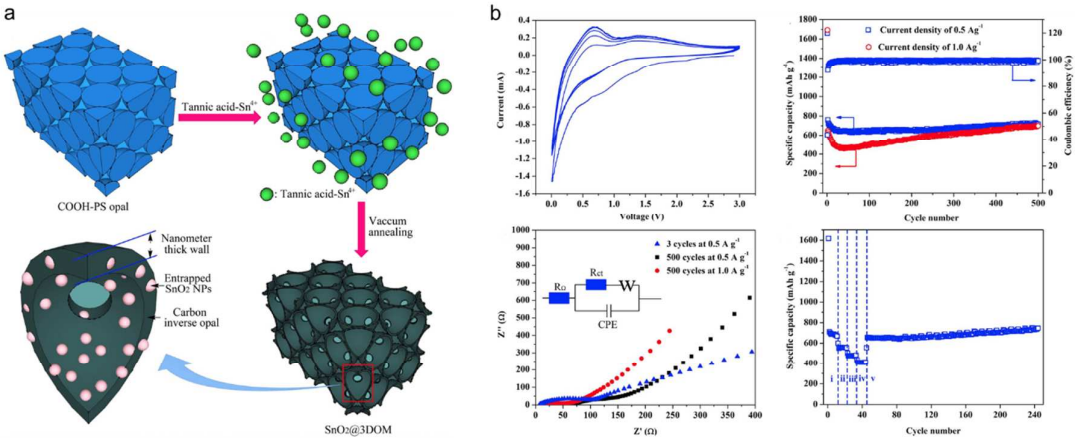

Figure 24 (a) Schematic illustration showing the preparation of SnO_2@C inverted opal electrode. (b) Li-ion battery performances of SnO_2@C inverse opal electrodes [90].

Development of such novel manufacturing techniques, optimization of the device configurations and improvement of the used materials will further enhance the performance of the supercapacitors, and we recommend recent reviews on this subject for more detailed

View Article Online
DOI: 10.1039/C4TA00534A

information. Developments in the area of ordered porous self-supported batteries with power densities comparable to supercapacitors offer power improvement options for materials that are fundamentally limited to low intercalative or non-faradaic charge capacities. Designing bi- or multi-phasic materials with different Li insertion voltage ranges could potentially allow for a predetermined capacity without fully discharging each active materials. Constraining one active materials within another with high deformation plasticity, could also potentially give a structurally stable matrix that better accommodated volumetric changes that are not buffered in a polymer-materials slurry in standard cell electrode designs. Recent findings in dual charge storage mechanisms using SnO_2 nanoparticles on Si as a hybrid anode [120] and their exploitation will help optimize tailored design of many other sophisticated electrode materials in electrochemistry and energy storage materials influenced by the end application.

Choosing pseudocapacitance and supercapacitance is also possible using two-dimensional (2D) nanosheets such as graphene or transition metal dichalcogenides (TMDCs) [220]. Charge storage mechanisms here involve the insertion/extraction of protons or ions in the first few nanometers on the surface of electrode materials for pseudocapacitors and the adsorption/desorption of ions at the electrode-electrolyte interface for electrochemical double-layer capacitors [221, 222]. Enhancing performance is again a function of reduced lithium ion diffusion distance within the materials if the former case and within the electrolyte for the latter case. With the boost of wearable and flexible consumer electronics that have an aesthetic appeal and unique functionality, flexibility and shape versatility or adaptability is a useful property in charge storage materials and their electrochemical cells [223-225]. The state-of-the-art flexible supercapacitors generally use carbon networks. Without the carbon networks pseudocapacitive materials can barely be used to fabricate the flexible electrodes,

View Article Online
DOI: 10.1039/C4TA00534A

so as to assemble the flexible supercapacitors (Fig. 25). Shi et al. [226], as one example, showed that flexible asymmetric supercapacitors with excellent electrochemical performance and in the form of quasi-transparent energy storage cells could be fabricated by using two kinds of ultrathin 2D nanosheet materials (MnO_2 and graphene). The 2 nm-thick MnO_2 nanosheets with a thickness of ~2 nm exhibited a high capacitance of 774 F g^{-1} and good rate performance. Flexible asymmetric supercapacitors using the ultrathin 2D MnO_2 and graphene in aqueous $Ca(NO_3)_2$-SiO_2 gel electrolyte realized excellent electrochemical performance with an energy density up to 97.2 Wh kg^{-1} much higher than traditional MnO_2 based supercapacitor and no more than 3% capacitance loss even after 10,000 cycles.

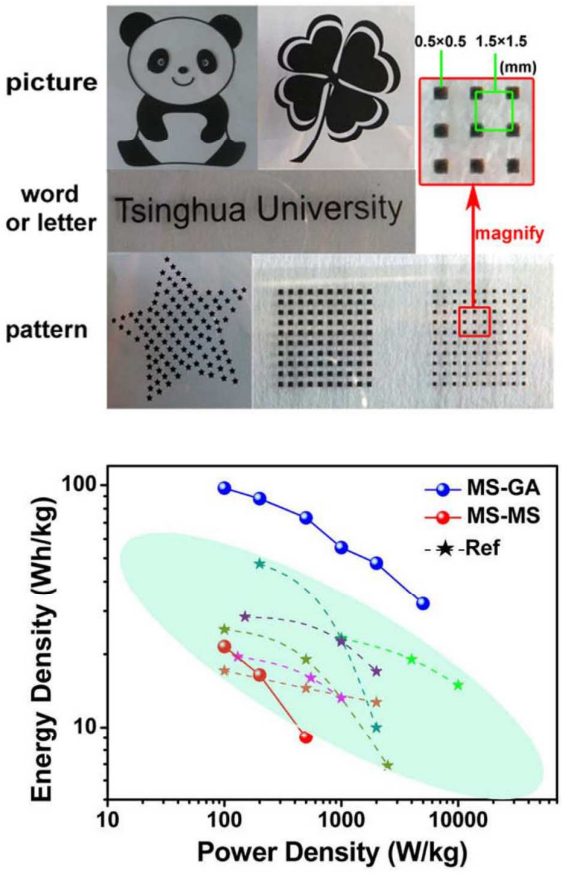

Figure 25 (a) Photographs of the screen-printed asymmetric nanosheets-based supercapacitor electrodes of various designs (b) Ragone plots of MS/GA and MS/MS supercapacitor compared with other MnO_2 based asymmetric supercapacitors in literature (based on the total mass of active materials).

View Article Online
DOI: 10.1039/C4TA00534A

10. Summary and outlook for energy storage material design and performance

In this review, a description of some of the recent advances in nanomaterials design, chemistry, size, shape, structure and assembly on the performance of Li-ion batteries was given. Particular focus was given to the influence of material parameters on cell performance and on emerging functional material architectures with engineered porosity as active Li-ion battery and pseudocapacitor materials. It is becoming clearer from the progress to date, that the improvements associated with changes of the electrode's chemical composition, combined with developments in electrode architecture offer excellent opportunities for commercialization of next generation Li-ion batteries and emerging alternative chemistries[227]. Various mechanisms for lithium storage combined with simple routes towards particular morphologies of active material create a multitude of opportunities for electrode design.

However, it is important to note that to date, only a handful of modern materials and electrode architectures have been commercialized. The advances in anode material science and design have not been followed to the same extent by improvements in the cathode chemistry and performance. A pressing challenge is the dearth of true, cell-level investigations of known and promising new materials in true Li-ion cells. Most cathode investigations form lithium batteries with a lithium electrodes; anode studies are half cells. While the fundamental advancements are motivating, many new materials and systems need to be thoroughly investigated using pair-matched anodes and cathodes in suitable electrodes as full Li-ion cells and classified for their optimum performance and loading conditions dictated by the end application.

View Article Online
DOI: 10.1039/C4TA00534A

Inverted opal architectures have been demonstrated to improve the performance of battery electrodes based on a variety of materials. The shortened diffusion lengths and excellent electrolyte infiltration allow for largely increased charge/discharge rates, while the void space allows for facile relaxation of strain and stress caused by repeated cycling of the electrode. Moreover, using a composite approach, where the inverted opal current collector acts as a support for active materials. This design approach can help minimize unwanted polarization and resistances, and achievement of outstanding charge/discharge rates. Such electrodes may achieve power densities more often seen in supercapacitors, while delivering energy densities characteristic for traditional LIBs. The use of engineered or programmed porosity is potentially very useful for materials that have inherently lower Li ion diffusivity within the crystal structure of the active material. Care should be taken to ensure that the structure of the porous network does not introduce significant increases in electrical resistance through material contacts or grain boundaries for example, or variable SEI film structure at anodes. Ideal scenarios would likely involve engineered porosity of a well crystallized material that itself does not have a high kinetic barrier to Li diffusion within its structure, made porous in a manner that maximizes ambipolar (ionic and electronic) conductivity (tuned for power or energy density requirements at a prescribed rate), forms stable SEI layers at low potentials (anodes), and offers useful volumetric or gravimetric energy densities, among other attributes. Recent efforts for some materials have shown that defining the porosity or dispersion of active materials can also give extra degrees of freedom for volume expansion common for many high capacity materials.

Ultimately, the successful application of materials chemistry and electrode design will be decided by the industry. Undoubtedly, the drive for better LIBs, motivated by automotive and consumer electronics market will have a dominating influence on the types of batteries

View Article Online
DOI: 10.1039/C4TA00534A

used. Templated materials with good ionic conductivities can allow for variants of thin film batteries, where the charge storage cell is designed around the shape of the electronic device, rather than the other way round. Although Li-ion battery packs are compact and volumetrically efficient, the 'swiss-roll' design strategy limits the batteries to rectangular or cylindrical shapes, which constrains the form factors of devices. While many factors need to be considered, not least a high quality, repeatable way of producing such thin film batteries and battery skins, scope exists to lay down energy storage cells in parallel with energy conversion or energy harvesting thin film technologies such as solar cells and thermoelectrics, on a single platform. Recent work on unconventional battery designs [228] focused on their accommodation into devices without constraining their form factors. Battery designs such as flexible batteries [229] stretchable paper-type batteries, and even printed transparent [230] batteries, show that such atypical batteries are possible. The use of IO materials is one way forward, allowing for possibilities of interpenetrating networks with Li-containing polymer electrolytes and sequentially layering of anode and protective encapsulating layers. Painting has proven its usefulness in applying functional materials onto almost any type of substrate for electronic devices and it may be applied to energy storage such as batteries. Printing (or generally, painting)[231] is already considered a viable technique for large-area fabrication of electronic devices (circuits, photovoltaics, displays, etc.) on virtually any type of substrate. Recent work has shown the intriguing possibility of literally painting the layers of materials required for a Li-ion battery [232].

For charge storage technology capable of high performance, faster charging, and stable, safe capacity retention during operation can be moulded to the device shape – this will significantly help advance portable device power technology options such as consumer devices and wireless sensor nodes for example. Consequently, there is huge interest in

View Article Online
DOI: 10.1039/C4TA00534A

developing a fully paintable energy storage technology, and a seamless integration of these energy storage systems into electronic devices is still a significant hurdle. Probing how an ordered architecture is that can be assembled layer-by-layer on shaped surfaces, and new non-destructive spectroscopic methods to investigate how a new areal battery shape can be probed during its operation will be very advantageous for future thin film, moldable battery designs and material architectures.

Advances in Li-air and Li-S designs and other 'beyond lithium' systems such as emerging Mg and Na-ion batteries [233, 234] might challenge the supremacy of the Li-ion system in the future, offering higher energy densities at reduced cost. Some investigations consider multivalent cations offering more than one electron per redox event. As summarised earlier, hybrid systems involving the power density benefits of supercapacitors and the energy density performance of batteries in the form of rate-dependent pseudocapacitors may also have niche application. However, for now, LIBs are very likely to remain the main solution for power systems, and thus drive further improvements in both electrode chemistry and architecture [235].

Acknowledgements

MO and EA acknowledge the support of the Irish Research Council under awards RS/2010/2920 and RS/2010/2170. COD acknowledges support from Science Foundation Ireland under award no. 07/SK/B1232a-STTF11, the UCC Strategic Research Fund, and from the Irish Research Council New Foundations Award. This research has also received funding from the Seventh Framework Programme FP7/2007-2013 (Project STABLE) under grant agreement n°314508.

View Article Online
DOI: 10.1039/C4TA00534A

References

1. W. S. Harris, PhD Thesis, University of California, 1958.
2. M. S. Whittingham, *Science*, 1976, **192**, 1126-1127.
3. M. S. Whittingham and R. A. Huggins, *The Journal of Chemical Physics*, 1971, **54**, 414-416.
4. B. Scrosati, *Journal of The Electrochemical Society*, 1992, **139**, 2776-2781.
5. W.-J. Zhang, *Journal of Power Sources*, 2011, **196**, 13-24.
6. R. Teki, M. K. Datta, R. Krishnan, T. C. Parker, T.-M. Lu, P. N. Kumta and N. Koratkar, *Small*, 2009, **5**, 2236-2242.
7. C.-M. Park, J.-H. Kim, H. Kim and H.-J. Sohn, *Chemical Society Reviews*, 2010, **39**, 3115-3141.
8. X.-P. Gao and H.-X. Yang, *Energy & Environmental Science*, 2010, **3**, 174-189.
9. Y. S. Cohen, Y. Cohen and D. Aurbach, *The Journal of Physical Chemistry B*, 2000, **104**, 12282-12291.
10. M. M. Thackeray, *Journal of The Electrochemical Society*, 1995, **142**, 2558-2563.
11. H. Shimotake, *Progress in Batteries and Solar Cells*, JEC Press, 1990.
12. O. C. Compton, A. Abouimrane, Z. An, M. J. Palmeri, L. C. Brinson, K. Amine and S. T. Nguyen, *Small*, 2012, **8**, 1110-1116.
13. B. Wang, J. Bates, F. Hart, B. Sales, R. Zuhr and J. Robertson, *Journal of The Electrochemical Society*, 1996, **143**, 3203-3213.
14. Y.-K. Sun, S.-T. Myung, B.-C. Park, J. Prakash, I. Belharouak and K. Amine, *Nature materials*, 2009, **8**, 320-324.
15. A. Manthiram and Y. Shin, Developments in Solid Oxide Fuel Cells and Lithium Iron Batteries: Proceedings of the 106th Annual Meeting of The American Ceramic Society, Indianapolis, Indiana, USA 2004, Ceramic Transactions, 2012.
16. L. Mai, L. Xu, C. Han, X. Xu, Y. Luo, S. Zhao and Y. Zhao, *Nano letters*, 2010, **10**, 4750-4755.
17. C. O'Dwyer, V. Lavayen, D. A. Tanner, S. B. Newcomb, E. Benavente, G. Gonzalez, E. Benavente and C. M. S. Torres, *Adv. Funct. Mater.*, 2009, **19**, 1736-1745
18. S. Dou, *Journal of Solid State Electrochemistry*, 2013, 1-16.
19. H. Pang, P. Cheng, H. Yang, J. Lu, C. X. Guo, G. Ning and C. M. Li, *Chemical Communications*, 2013, **49**, 1536-1538.
20. M. M. Thackeray, W. I. F. David, P. G. Bruce and J. B. Goodenough, *Materials Research Bulletin*, 1983, **18**, 461-472.
21. K. Xu, *Chemical Reviews*, 2004, **104**, 4303-4418.
22. M. D. Bhatt and C. O'Dwyer, *Curr. Appl. Phys.*, 2014, **14**, 349-354.
23. L. El Ouatani, R. Dedryvère, C. Siret, P. Biensan and D. Gonbeau, *Journal of The Electrochemical Society*, 2009, **156**, A468-A477.
24. E. Peled, *Journal of The Electrochemical Society*, 1979, **126**, 2047-2051.
25. J. O. Besenhard, M. Winter, J. Yang and W. Biberacher, *Journal of Power Sources*, 1995, **54**, 228-231.
26. V. Nicolosi, M. Chhowalla, M. G. Kanatzidis, M. S. Strano and J. N. Coleman, *Science*, 2013, **340**, 1226419.
27. M. Chhowalla, H. S. Shin, G. Eda, L.-J. Li, K. P. Loh and H. Zhang, *Nat. Chem.*, 2013, **5**, 263-275.
28. J. N. Coleman, M. Lotya, A. O'Neill, S. D. Bergin, P. J. King, U. Khan, K. Young, A. Gaucher, S. De, R. J. Smith, I. V. Shvets, S. K. Arora, G. Stanton, H.-Y. Kim, K. Lee, G. T. Kim, G. S. Duesberg, T. Hallam, J. J. Boland, J. J. Wang, J. F. Donegan, J. C. Grunlan, G. Moriarty, A. Shmeliov, R. J. Nicholls, J. M. Perkins, E. M. Grieveson, K. Theuwissen, D. W. McComb, P. D. Nellist and V. Nicolosi, *Science*, 2011, **331**, 568-571.
29. P. Poizot, S. Laruelle, S. Grugeon, L. Dupont and J. M. Tarascon, *Nature*, 2000, **407**, 496-499.
30. J. M. Haag, G. Pattanaik and M. F. Durstock, *Advanced Materials*, 2013, **25**, 3238-3243.
31. J. B. Goodenough and Y. Kim, *Chemistry of Materials*, 2009, **22**, 587-603.

View Article Online
DOI: 10.1039/C4TA00534A

32. L. Su, Y. Jing and Z. Zhou, *Nanoscale*, 2011, **3**, 3967-3983.
33. A. Jain, S. P. Ong, G. Hautier, W. Chen, W. D. Richards, S. Dacek, S. Cholia, D. Gunter, D. Skinner, G. Ceder and K. A. Persson, *APL Materials*, 2013, **1**, -.
34. M. J. Armstrong, C. O'Dwyer, W. J. Macklin and J. D. Holmes, *Nano Res.*, 2014, **7**, 1-62.
35. G. Ceder, *MRS Bull.*, 2010, **35**.
36. K. Mizushima, P. C. Jones, P. J. Wiseman and J. B. Goodenough, *Materials Research Bulletin*, 1980, **15**, 783-789.
37. B. Kang and G. Ceder, *Nature*, 2009, **458**, 190-193.
38. S.-Y. Chung, J. T. Bloking and Y.-M. Chiang, *Nature Materials*, 2002, **1**, 123-128.
39. E. Hosono, T. Kudo, I. Honma, H. Matsuda and H. S. Zhou, *Nano Letters*, 2009, **9**, 1045-1051.
40. J. Molenda, S. J, M. K, O. W, Z. M, M. M, D. M and D. R, *Solid State Ionics*, 2004, **171**, 215.
41. S. Dou, *Journal of Solid State Electrochemistry*, 2013, **17**, 911-926.
42. J. Molenda, P. Wilk and J. Marzec, *Solid State Ionics*, 2002, **146**, 73-79.
43. A. Heller, *Interface*, 2013, **22**, 35.
44. M. Jacoby, *Chemical and Engineering News*, 2013, **91**, 7.
45. Y. S. Hu, L. Kienle, Y. G. Guo and J. Maier, *Advanced Materials*, 2006, **18**, 1421-+.
46. Y.-G. Guo, J.-S. Hu and L.-J. Wan, *Advanced Materials*, 2008, **20**, 2878-2887.
47. B. L. Ellis, K. T. Lee and L. F. Nazar, *Chemistry of Materials*, 2010, **22**, 691-714.
48. B. Kang and G. Ceder, *Nature*, 2009, **458**, 190-193.
49. Y. G. Wang, Y. R. Wang, E. J. Hosono, K. X. Wang and H. S. Zhou, *Angew. Chem. Int. Ed.*, 2008, **47**, 7461–7465.
50. S. Suzuki and M. Miyayama, *Journal of The Electrochemical Society*, 2013, **160**, A293-A296.
51. D. Burch and M. Z. Bazant, *Nano Letters*, 2009, **9**, 3795-3800.
52. A. R. Armstrong, G. Armstrong, J. Canales and P. G. Bruce, *Angewandte Chemie International Edition*, 2004, **43**, 2286-2288.
53. H. Shimoda, B. Gao, X. P. Tang, A. Kleinhammes, L. Fleming, Y. Wu and O. Zhou, *Phys Rev Lett*, 2002, **88**, 015502.
54. J. Molenda and M. Molenda, *Composite Cathode Material for Li-Ion Batteries Based on LiFePO4 System*, 2011.
55. P. Poizot, S. Laruelle, S. Grugeon, L. Dupont and J.-M. Tarascon, *Nature*, 2000, **407**, 496-499.
56. J. Cabana, L. Monconduit, D. Larcher and M. R. Palacín, *Advanced Materials*, 2010, **22**, E170-E192.
57. A. N. Dey, *Journal of The Electrochemical Society*, 1971, **118**, 1547-1549.
58. J. S. Chen and X. W. Lou, *Small*, 2013, **9**, 1877-1893.
59. Z. Chen, Y. Cao, J. Qian, X. Ai and H. Yang, *Journal of Physical Chemistry C*, 2010, **114**, 15196-15201.
60. C. K. Chan, X. F. Zhang and Y. Cui, *Nano Letters*, 2008, **8**, 307-309.
61. W. Wang, P. Li, Y. Fu and X. Ma, *Journal of Power Sources*, 2013, **238**, 464-468.
62. S. J. R. Prabakar, Y.-H. Hwang, E.-G. Bae, S. Shim, D. Kim, M. S. Lah, K.-S. Sohn and M. Pyo, *Advanced Materials*, 2013, **25**, 3307-3312.
63. J. Kong, W. A. Yee, Y. Wei, L. Yang, J. M. Ang, S. L. Phua, S. Y. Wong, R. Zhou, Y. Dong, X. Li and X. Lu, *Nanoscale*, 2013, **5**, 2967-2973.
64. Q. Guo, Z. Zheng, H. Gao, J. Ma and X. Qin, *Journal of Power Sources*, 2013, **240**, 149-154.
65. U. Kasavajjula, C. Wang and A. J. Appleby, *Journal of Power Sources*, 2007, **163**, 1003-1039.
66. H. Wu, G. Chan, J. W. Choi, I. Ryu, Y. Yao, M. T. McDowell, S. W. Lee, A. Jackson, Y. Yang, L. Hu and Y. Cui, *Nature Nanotechnology*, 2012, **7**, 309-314.
67. C. K. Chan, H. Peng, G. Liu, K. McIlwrath, X. F. Zhang, R. A. Huggins and Y. Cui, *Nature Nanotechnology*, 2008, **3**, 31-35.
68. W. McSweeney, O. Lotty, N. V. V. Mogili, C. Glynn, H. Geaney, D. Tanner, J. D. Holmes and C. O'Dwyer, *J. Appl. Phys.*, 2013, **114**, 034309.

View Article Online
DOI: 10.1039/C4TA00534A

69. N. Liu, H. Wu, M. T. McDowell, Y. Yao, C. Wang and Y. Cui, *Nano Letters*, 2012, **12**, 3315-3321.
70. X. H. Liu, H. Zheng, L. Zhong, S. Huan, K. Karki, L. Q. Zhang, Y. Liu, A. Kushima, W. T. Liang, J. W. Wang, J.-H. Cho, E. Epstein, S. A. Dayeh, S. T. Picraux, T. Zhu, J. Li, J. P. Sullivan, J. Cumings, C. Wang, S. X. Mao, Z. Z. Ye, S. Zhang and J. Y. Huang, *Nano Letters*, 2011, **11**, 3312-3318.
71. T.-L. Chan and J. R. Chelikowsky, *Nano Letters*, 2010, **10**, 821-825.
72. X. H. Liu, F. Fan, H. Yang, S. Zhang, J. Y. Huang and T. Zhu, *Acs Nano*, 2013, **7**, 1495-1503.
73. J. W. Wang, Y. He, F. Fan, X. H. Liu, S. Xia, Y. Liu, C. T. Harris, H. Li, J. Y. Huang, S. X. Mao and T. Zhu, *Nano Letters*, 2013, **13**, 709-715.
74. K. Peng, J. Jie, W. Zhang and S.-T. Lee, *Applied Physics Letters*, 2008, **93**.
75. S. D. Beattie, D. Larcher, M. Morcrette, B. Simon and J. M. Tarascon, *Journal of the Electrochemical Society*, 2008, **155**, A158-A163.
76. A. M. Chockla, T. D. Bogart, C. M. Hessel, K. C. Klavetter, C. B. Mullins and B. A. Korgel, *The Journal of Physical Chemistry C*, 2012, **116**, 18079-18086.
77. A. M. Chockla, K. C. Klavetter, C. B. Mullins and B. A. Korgel, *Chemistry of Materials*, 2012, **24**, 3738-3745.
78. E. Mullane, T. Kennedy, H. Geaney, C. Dickinson and K. M. Ryan, *Chemistry of Materials*, 2013, **25**, 1816-1822.
79. C. K. Chan, R. N. Patel, M. J. O'Connell, B. A. Korgel and Y. Cui, *Acs Nano*, 2010, **4**, 1443-1450.
80. J. K. Lee, K. B. Smith, C. M. Hayner and H. H. Kung, *Chemical Communications*, 2010, **46**, 2025-2027.
81. J. Guo, A. Sun and C. Wang, *Electrochemistry Communications*, 2010, **12**, 981-984.
82. J. Guo, X. Chen and C. Wang, *Journal of Materials Chemistry*, 2010, **20**, 5035-5040.
83. S.-L. Chou, Y. Zhao, J.-Z. Wang, Z.-X. Chen, H.-K. Liu and S.-X. Dou, *Journal of Physical Chemistry C*, 2010, **114**, 15862-15867.
84. H. Kim and J. Cho, *Nano Letters*, 2008, **8**, 3688-3691.
85. L.-F. Cui, L. Hu, J. W. Choi and Y. Cui, *Acs Nano*, 2010, **4**, 3671-3678.
86. H. Guan, X. Wang, S. Chen, Y. Bando and D. Golberg, *Chemical Communications*, 2011, **47**, 12098-12100.
87. K. Evanoff, A. Magasinski, J. Yang and G. Yushin, *Advanced Energy Materials*, 2011, **1**, 495-498.
88. W. Wang and P. N. Kumta, *Acs Nano*, 2010, **4**, 2233-2241.
89. L. Su, Z. Zhou and M. Ren, *Chemical Communications*, 2010, **46**, 2590-2592.
90. X. Huang, J. Chen, Z. Lu, H. Yu, Q. Yan and H. H. Hng, *Scientific Reports*, 2013, **3**.
91. Y.-S. Hu, R. Demir-Cakan, M.-M. Titirici, J.-O. Mueller, R. Schloegl, M. Antonietti and J. Maier, *Angewandte Chemie-International Edition*, 2008, **47**, 1645-1649.
92. H. Kim, B. Han, J. Choo and J. Cho, *Angewandte Chemie-International Edition*, 2008, **47**, 10151-10154.
93. L.-F. Cui, Y. Yang, C.-M. Hsu and Y. Cui, *Nano Letters*, 2009, **9**, 3370-3374.
94. R. Huang, X. Fan, W. Shen and J. Zhu, *Applied Physics Letters*, 2009, **95**.
95. M.-H. Park, M. G. Kim, J. Joo, K. Kim, J. Kim, S. Ahn, Y. Cui and J. Cho, *Nano Letters*, 2009, **9**, 3844-3847.
96. S.-L. Chou, J.-Z. Wang, M. Choucair, H.-K. Liu, J. A. Stride and S.-X. Dou, *Electrochemistry Communications*, 2010, **12**, 303-306.
97. K. Kang, H.-S. Lee, D.-W. Han, G.-S. Kim, D. Lee, G. Lee, Y.-M. Kang and M.-H. Jo, *Applied Physics Letters*, 2010, **96**.
98. A. Magasinski, P. Dixon, B. Hertzberg, A. Kvit, J. Ayala and G. Yushin, *Nature Materials*, 2010, **9**, 353-358.

View Article Online
DOI: 10.1039/C4TA00534A

99. T. Song, J. Xia, J.-H. Lee, D. H. Lee, M.-S. Kwon, J.-M. Choi, J. Wu, S. K. Doo, H. Chang, W. Il Park, D. S. Zang, H. Kim, Y. Huang, K.-C. Hwang, J. A. Rogers and U. Paik, *Nano Letters*, 2010, **10**, 1710-1716.
100. F.-F. Cao, J.-W. Deng, S. Xin, H.-X. Ji, O. G. Schmidt, L.-J. Wan and Y.-G. Guo, *Advanced Materials*, 2011, **23**, 4415-+.
101. M. Ge, J. Rong, X. Fang and C. Zhou, *Nano Letters*, 2012, **12**, 2318-2323.
102. J. Graetz, C. C. Ahn, R. Yazami and B. Fultz, *Journal of The Electrochemical Society*, 2004, **151**, A698-A702.
103. A. M. Chockla, J. T. Harris, V. A. Akhavan, T. D. Bogart, V. C. Holmberg, C. Steinhagen, C. B. Mullins, K. J. Stevenson and B. A. Korgel, *Journal of the American Chemical Society*, 2011, **133**, 20914-20921.
104. G. Cui, L. Gu, L. Zhi, N. Kaskhedikar, P. A. van Aken, K. Muellen and J. Maier, *Advanced Materials*, 2008, **20**, 3079-3083.
105. B. Laforge, L. Levan-Jodin, R. Salot and A. Billard, *Journal of the Electrochemical Society*, 2008, **155**, A181-A188.
106. L. C. Yang, Q. S. Gao, L. Li, Y. Tang and Y. P. Wu, *Electrochemistry Communications*, 2010, **12**, 418-421.
107. M.-H. Park, Y. Cho, K. Kim, J. Kim, M. Liu and J. Cho, *Angewandte Chemie-International Edition*, 2011, **50**, 9647-9650.
108. S. Yoon, C.-M. Park and H.-J. Sohn, *Electrochemical and Solid State Letters*, 2008, **11**, A42-A45.
109. D.-J. Xue, S. Xin, Y. Yan, K.-C. Jiang, Y.-X. Yin, Y.-G. Guo and L.-J. Wan, *Journal of the American Chemical Society*, 2012, **134**, 2512-2515.
110. K. H. Seng, M.-H. Park, Z. P. Guo, H. K. Liu and J. Cho, *Angewandte Chemie-International Edition*, 2012, **51**, 5657-5661.
111. A. M. Chockla, M. G. Panthani, V. C. Holmberg, C. M. Hessel, D. K. Reid, T. D. Bogart, J. T. Harris, C. B. Mullins and B. A. Korgel, *Journal of Physical Chemistry C*, 2012, **116**, 11917-11923.
112. M.-H. Seo, M. Park, K. T. Lee, K. Kim, J. Kim and J. Cho, *Energy & Environmental Science*, 2011, **4**, 425-428.
113. Y. Hwa, C.-M. Park, S. Yoon and H.-J. Sohn, *Electrochimica Acta*, 2010, **55**, 3324-3329.
114. J. Wang, N. Du, H. Zhang, J. Yu and D. Yang, *Journal of Materials Chemistry*, 2012, **22**, 1511-1515.
115. I. A. Courtney and J. R. Dahn, *Journal of the Electrochemical Society*, 1997, **144**, 2045-2052.
116. Y. Idota, T. Kubota, A. Matsufuji, Y. Maekawa and T. Miyasaka, *Science*, 1997, **276**, 1395-1397.
117. X. H. Liu and J. Y. Huang, *Energy & Environmental Science*, 2011, **4**, 3844-3860.
118. M. Gu, Z. Wang, J. G. Connell, D. E. Perea, L. J. Lauhon, F. Gao and C. Wang, *ACS nano*, 2013, **7**, 6303-6309.
119. J. S. Chen and X. W. Lou, *Materials Today*, 2012, **15**, 246-254.
120. M. Osiak, E. Armstrong, T. Kennedy, C. M. S. Torres, K. M. Ryan and C. O'Dwyer, *ACS Appl. Mater. Interfaces*, 2013, **5**, 8195–8202.
121. D.-W. Kim, I.-S. Hwang, S. J. Kwon, H.-Y. Kang, K.-S. Park, Y.-J. Choi, K.-J. Choi and J.-G. Park, *Nano Letters*, 2007, **7**, 3041-3045.
122. G. Du, C. Zhong, P. Zhang, Z. Guo, Z. Chen and H. Liu, *Electrochimica Acta*, 2010, **55**, 2582-2586.
123. K. K. D. Ehinon, S. Naille, R. Dedryvere, P. E. Lippens, J. C. Jumas and D. Gonbeau, *Chemistry of Materials*, 2008, **20**, 5388-5398.
124. J. Hassoun, P. Ochal, S. Panero, G. Mulas, C. B. Minella and B. Scrosati, *Journal of Power Sources*, 2008, **180**, 568-575.

View Article Online
DOI: 10.1039/C4TA00534A

125. J.-W. Seo, J.-t. Jang, S.-W. Park, C. Kim, B. Park and J. Cheon, *Advanced Materials*, 2008, **20**, 4269-4273.
126. Z. Chen, J. Qian, X. Ai, Y. Cao and H. Yang, *Journal of Power Sources*, 2009, **189**, 730-732.
127. D. Deng, M. G. Kim, J. Y. Lee and J. Cho, *Energy & Environmental Science*, 2009, **2**, 818-837.
128. X.-Y. Fan, F.-S. Ke, G.-Z. Wei, L. Huang and S.-G. Sun, *Journal of Alloys and Compounds*, 2009, **476**, 70-73.
129. R. Z. Hu, M. Q. Zeng and M. Zhu, *Electrochimica Acta*, 2009, **54**, 2843-2850.
130. L. Trahey, J. T. Vaughey, H. H. Kung and M. M. Thackeray, *Journal of the Electrochemical Society*, 2009, **156**, A385-A389.
131. J. Hassoun and B. Scrosati, *Angewandte Chemie-International Edition*, 2010, **49**, 2371-2374.
132. G. F. Ortiz, I. Hanzu, P. Lavela, P. Knauth, J. L. Tirado and T. Djenizian, *Chemistry of Materials*, 2010, **22**, 1926-1932.
133. L. Xue, Z. Fu, Y. Yao, T. Huang and A. Yu, *Electrochimica Acta*, 2010, **55**, 7310-7314.
134. J. S. Chen, L. A. Archer and X. W. Lou, *Journal of Materials Chemistry*, 2011, **21**, 9912-9924.
135. J. Yan, A. Sumboja, E. Khoo and P. S. Lee, *Advanced Materials*, 2011, **23**, 746-+.
136. Y.-C. Chen, T.-F. Hung, C.-W. Hu, C.-Y. Chiang, C.-W. Huang, H.-C. Su, R.-S. Liu, C.-H. Lee and C.-C. Chang, *Nanoscale*, 2013, **5**, 2254-2258.
137. F. S. Ke, L. Huang, H. H. Jiang, H. B. Wei, F. Z. Yang and S. G. Sun, *Electrochemistry Communications*, 2007, **9**, 228-232.
138. X. J. Zhu, Z. P. Guo, P. Zhang, G. D. Du, R. Zeng, Z. X. Chen, S. Li and H. K. Liu, *Journal of Materials Chemistry*, 2009, **19**, 8360-8365.
139. J. R. Dahn, R. E. Mar and A. Abouzeid, *Journal of The Electrochemical Society*, 2006, **153**, A361-A365.
140. M. G. Kim and J. Cho, *Journal of the Electrochemical Society*, 2009, **156**, A277-A282.
141. L. Q. Zhang, X. H. Liu, Y.-C. Perng, J. Cho, J. P. Chang, S. X. Mao, Z. Z. Ye and J. Y. Huang, *Micron*, 2012, **43**, 1127-1133.
142. Y.-J. Chen, C.-L. Zhu, X.-Y. Xue, X.-L. Shi and M.-S. Cao, *Applied Physics Letters*, 2008, **92**.
143. Z. Wang, G. Chen and D. Xia, *Journal of Power Sources*, 2008, **184**, 432-436.
144. D. Deng and J. Y. Lee, *Angewandte Chemie-International Edition*, 2009, **48**, 1660-1663.
145. S.-M. Paek, E. Yoo and I. Honma, *Nano Letters*, 2009, **9**, 72-75.
146. Y. Yu, L. Gu, C. Wang, A. Dhanabalan, P. A. van Aken and J. Maier, *Angewandte Chemie-International Edition*, 2009, **48**, 6485-6489.
147. Y. Yu, L. Gu, X. Lang, C. Zhu, T. Fujita, M. Chen and J. Maier, *Advanced Materials*, 2011, **23**, 2443-+.
148. V. Subramanian, W. W. Burke, H. Zhu and B. Wei, *Journal of Physical Chemistry C*, 2008, **112**, 4550-4556.
149. P. Meduri, C. Pendyala, V. Kumar, G. U. Sumanasekera and M. K. Sunkara, *Nano Letters*, 2009, **9**, 612-616.
150. J. S. Chen, Y. L. Cheah, Y. T. Chen, N. Jayaprakash, S. Madhavi, Y. H. Yang and X. W. Lou, *Journal of Physical Chemistry C*, 2009, **113**, 20504-20508.
151. R. Demir-Cakan, Y.-S. Hu, M. Antonietti, J. Maier and M.-M. Titirici, *Chemistry of Materials*, 2008, **20**, 1227-1229.
152. B. Guo, J. Shu, K. Tang, Y. Bai, Z. Wang and L. Chen, *Journal of Power Sources*, 2008, **177**, 205-210.
153. H. Kim and J. Cho, *Journal of Materials Chemistry*, 2008, **18**, 771-775.
154. C. Wang, Y. Zhou, M. Ge, X. Xu, Z. Zhang and J. Z. Jiang, *Journal of the American Chemical Society*, 2010, **132**, 46-+.
155. X. Li, A. Dhanabalan, L. Gu and C. Wang, *Advanced Energy Materials*, 2012, **2**, 238-244.
156. B. Luo, B. Wang, M. Liang, J. Ning, X. Li and L. Zhi, *Advanced Materials*, 2012, **24**, 1405-1409.
157. *Sony update its Nexelion Batteries with the new 3.5Ah 18650WH1*, Accessed 08.10, 2013.
158. D. Foster, J. Wolfenstine, J. Read and J. L. Allen, *Army Research Laboratory*, 2008, **June 2008**.

View Article Online
DOI: 10.1039/C4TA00534A

159. C. Capiglia, Y. Saito, H. Kageyama, P. Mustarelli, T. Iwamoto, T. Tabuchi and H. Tukamoto, *Journal of Power Sources*, 1999, **81–82**, 859-862.
160. A. Vu, Y. Qian and A. Stein, *Advanced Energy Materials*, 2012, **2**, 1056-1085.
161. N. Krins, J. D. Bass, D. Grosso, C. Henrist, R. Delaigle, E. M. Gaigneaux, R. Cloots, B. Vertruyen and C. Sanchez, *Chemistry of Materials*, 2011, **23**, 4124-4131.
162. J. J. Schneider and J. Engstler, *European Journal of Inorganic Chemistry*, 2006, **2006**, 1723-1736.
163. K. Wang, M. Wei, M. A. Morris, H. Zhou and J. D. Holmes, *Advanced Materials*, 2007, **19**, 3016-3020.
164. F. Cheng, Z. Tao, J. Liang and J. Chen, *Chemistry of Materials*, 2007, **20**, 667-681.
165. Y. Ren, L. J. Hardwick and P. G. Bruce, *Angewandte Chemie International Edition*, 2010, **49**, 2570-2574.
166. F. Jiao and P. G. Bruce, *Advanced Materials*, 2007, **19**, 657-+.
167. J. M. Kim, Y. S. Huh, Y.-K. Han, M. S. Cho and H. J. Kim, *Electrochemistry Communications*, 2012, **14**, 32-35.
168. L. Dupont, S. Laruelle, S. Grugeon, C. Dickinson, W. Zhou and J. M. Tarascon, *Journal of Power Sources*, 2008, **175**, 502-509.
169. L. Tian, H. Zou, J. Fu, X. Yang, Y. Wang, H. Guo, X. Fu, C. Liang, M. Wu, P. K. Shen and Q. Gao, *Advanced Functional Materials*, 2010, **20**, 617-623.
170. K. Shiva, S. Asokan and A. J. Bhattacharyya, *Nanoscale*, 2011, **3**, 1501-1503.
171. H. Liu, G. Wang, J. Liu, S. Qiao and H. Ahn, *Journal of Materials Chemistry*, 2011, **21**, 3046-3052.
172. N. D. Petkovich and A. Stein, *Chemical Society Reviews*, 2013, **42**, 3721-3739.
173. E. Armstrong, W. Khunsin, M. Osiak, M. Blömker, C. M. S. Torres and C. O'Dwyer, *Small*, 2014 DOI:10.1002/smll.201303616.
174. A. Stein, B. E. Wilson and S. G. Rudisill, *Chemical Society Reviews*, 2013, **42**, 2763-2803.
175. M. Osiak, E. Armstrong and C. O'Dwyer, *ECS Trans.*, 2013, **53**, 85-91.
176. D.-l. Ma, Z.-y. Cao, H.-g. Wang, X.-l. Huang, L.-m. Wang and X.-b. Zhang, *Energy & Environmental Science*, 2012, **5**, 8538-8542.
177. G. Collins, M. Blomker, M. Osiak, J. D. Holmes, M. Bredol and C. O'Dwyer, *Chem. Mater.*, 2013, **25**, 4312 - 4320.
178. J. S. Sakamoto and B. Dunn, *Journal of Materials Chemistry*, 2002, **12**, 2859-2861.
179. L. Li, U. Steiner and S. Mahajan, *Journal of Materials Chemistry*, 2010, **20**, 7131-7134.
180. N. S. Ergang, J. C. Lytle, H. Yan and A. Stein, *Journal of The Electrochemical Society*, 2005, **152**, A1989-A1995.
181. H. Yan, S. Sokolov, J. C. Lytle, A. Stein, F. Zhang and W. H. Smyrl, *Journal of The Electrochemical Society*, 2003, **150**, A1102-A1107.
182. Q. Qu, L. Fu, X. Zhan, D. Samuelis, J. Maier, L. Li, S. Tian, Z. Li and Y. Wu, *Energy & Environmental Science*, 2011, **4**, 3985-3990.
183. A. K. Padhi, K. S. Nanjundaswamy and J. B. Goodenough, *Journal of The Electrochemical Society*, 1997, **144**, 1188-1194.
184. J. Lu, Z. Tang, Z. Zhang and W. Shen, *Materials Research Bulletin*, 2005, **40**, 2039-2046.
185. C. M. Doherty, R. A. Caruso, B. M. Smarsly and C. J. Drummond, *Chemistry of Materials*, 2009, **21**, 2895-2903.
186. A. A. Zakhidov, R. H. Baughman, Z. Iqbal, C. Cui, I. Khayrullin, S. O. Dantas, J. Marti and V. G. Ralchenko, *Science*, 1998, **282**, 897-901.
187. J.-S. Yu, S. Kang, S. B. Yoon and G. Chai, *Journal of the American Chemical Society*, 2002, **124**, 9382-9383.
188. K. T. Lee, J. C. Lytle, N. S. Ergang, S. M. Oh and A. Stein, *Advanced Functional Materials*, 2005, **15**, 547-556.

View Article Online
DOI: 10.1039/C4TA00534A

189. F. B. Su, X. S. Zhao, Y. Wang, J. H. Zeng, Z. C. Zhou and J. Y. Lee, *Journal of Physical Chemistry B*, 2005, **109**, 20200-20206.
190. D.-Y. Kang, S.-O. Kim, Y. J. Chae, J. K. Lee and J. H. Moon, *Langmuir*, 2013, **29**, 1192-1198.
191. Z. Wang, F. Li, N. S. Ergang and A. Stein, *Carbon*, 2008, **46**, 1702-1710.
192. Z. Y. Wang, N. S. Ergang, M. A. Al-Daous and A. Stein, *Chemistry of Materials*, 2005, **17**, 6805-6813.
193. A. Stein, *Nat. Nanotechnol.*, 2011, **6**, 262-263.
194. J. C. Lytle, H. W. Yan, N. S. Ergang, W. H. Smyrl and A. Stein, *Journal of Materials Chemistry*, 2004, **14**, 1616-1622.
195. Z. Wang, M. A. Fierke and A. Stein, *Journal of the Electrochemical Society*, 2008, **155**, A658-A663.
196. K. Nishikawa, K. Dokko, K. Kinoshita, S.-W. Woo and K. Kanamura, *Journal of Power Sources*, 2009, **189**, 726-729.
197. F.-Q. Liu, H. Wu, T. Li, L. R. Grabstanowicz, K. Amine and T. Xu, *Nanoscale*, 2013, **5**, 6422-6429.
198. A. Esmanski and G. A. Ozin, *Advanced Functional Materials*, 2009, **19**, 1999-2010.
199. H. Zhang and P. V. Braun, *Nano Letters*, 2012, **12**, 2778-2783.
200. H. Zhang, X. Yu and P. V. Braun, *Nature Nanotechnology*, 2011, **6**, 277-281.
201. J. H. Pikul, H. Gang Zhang, J. Cho, P. V. Braun and W. P. King, *Nat Commun*, 2013, **4**, 1732.
202. J. W. Long, B. Dunn, D. R. Rolison and H. S. White, *Chemical Reviews*, 2004, **104**, 4463-4492.
203. Z. Bing, Y. Yuan, Y. Wang and Z. W. Fu, *Electrochemical and Solid State Letters*, 2006, **9**, A101-A104.
204. E. M. Sorensen, S. J. Barry, H. K. Jung, J. R. Rondinelli, J. T. Vaughey and K. R. Poeppelmeier, *Chemistry of Materials*, 2006, **18**, 482-489.
205. S.-W. Woo, K. Dokko and K. Kanamura, *Electrochimica Acta*, 2007, **53**, 79-82.
206. W.-j. Cui, H.-j. Liu, C.-x. Wang and Y.-y. Xia, *Electrochemistry Communications*, 2008, **10**, 1587-1589.
207. H. Nakano, K. Dokko, M. Hara, Y. Isshiki and K. Kanamura, *Ionics*, 2008, **14**, 173-177.
208. D. Tonti, M. J. Torralvo, E. Enciso, I. Sobrados and J. Sanz, *Chemistry of Materials*, 2008, **20**, 4783-4790.
209. H. Jiang, X. Yang, C. Chen, Y. Zhu and C. Li, *New Journal of Chemistry*, 2013, **37**, 1578-1583.
210. J. R. Miller and P. Simon, *Science*, 2008, **321**, 651-652.
211. B. E. Conway, *Electrochim. Acta*, 1993, **38**, 1249-1258.
212. B. E. Conway, *J. Electrochem. Soc.*, 1991, **138**, 1539-1548.
213. J. Wang, J. Polleux, J. Lim and B. Dunn, *The Journal of Physical Chemistry C*, 2007, **111**, 14925-14931.
214. H. Lindström, S. Södergren, A. Solbrand, H. Rensmo, J. Hjelm, A. Hagfeldt and S.-E. Lindquist, *The Journal of Physical Chemistry B*, 1997, **101**, 7717-7722.
215. T. Brezesinski, J. Wang, S. H. Tolbert and B. Dunn, *Nat. Mater.*, 2010, **9**, 146-151.
216. A. Vu, Y. Q. Qian and A. Stein, *Adv. Energy Mater.* , 2012, **2**, 1056-1085.
217. M. Zukalova, *Chem. Mater.*, 2005, **17**, 1248-1255.
218. J. R. Li, Z. L. Tang and Z. T. Zhang, *Chem. Phys. Lett.*, 2006, **418**, 506-510.
219. H. B. Li, M. H. Yu, F. X. Wang, P. Liu, Y. Liang, J. Xiao, C. X. Wang, Y. X. Tong and G. W. Yang, *Nature Communications*, 2013, **4**.
220. M. D. Stoller, S. Park, Y. Zhu, J. An and R. S. Ruoff, *Nano Lett.*, 2008, **8**, 3498-3502.
221. M. Toupin, T. Brousse and D. Belanger, *Chem.Mater.*, 2004, **16**, 3184-3190.
222. P. Simon and Y. Gogotsi, *Nat. Mater.*, 2008, **7**, 845-854.
223. M. F. El-Kady, V. Strong, S. Dubin and R. B. Kaner, *Science*, 2012, **335**, 1326-1330.
224. L. Hu and Y. Cui, *Energy Environ. Sci.*, 2012, **5**, 6423-6435.
225. S. Y. Lee, K.-H. Choi, W.-S. Choi, Y. H. Kwon, H.-R. Jung, H.-C. Shin and J. Y. Kim, *Energy Environ. Sci.*, 2013, **6**, 2414-2423.

View Article Online
DOI: 10.1039/C4TA00534A

226. S. Shi, C. Xu, C. Yang, Y. Chen, J. Liu and F. Kang, *Sci. Rep.*, 2013, **3**, 2598.
227. T. Kennedy, E. Mullane, H. Geaney, M. Osiak, C. O'Dwyer and K. M. Ryan, *Nano Lett.*, 2014, **14** 716-723.
228. B. L. Spare, U. S. P. Office, Ed. (Apple Inc.) *United States Pat.*, 2012.
229. H. Nishide and K. Oyaizu, *Science*, 2008, **319**, 737-738.
230. Y. Yang, S. Jeong, L. Hu, H. Wu, S. W. Lee and Y. Cui, *Proceedings of the National Academy of Sciences*, 2011, **108**, 13013-13018.
231. N. Singh, C. Galande, A. Miranda, A. Mathkar, W. Gao, A. L. Mohana Reddy, A. Vlad and P. M. Ajayan, *Sci. Rep.*, 2012, **2**, 481.
232. N. Singh, C. Galande, A. Miranda, A. Mathkar, W. Gao, A. L. M. Reddy, A. Vlad and P. M. Ajayan, *Scientific Reports*, 2012, **2**.
233. V. Palomares, P. Serras, I. Villaluenga, K. B. Hueso, J. Carretero-Gonzalez and T. Rojo, *Energy & Environmental Science*, 2012, **5**, 5884-5901.
234. B. Liu, T. Luo, G. Mu, X. Wang, D. Chen and G. Shen, *ACS Nano*, 2013, **7**, 8051-8058.
235. B. Scrosati and J. Garche, *Journal of Power Sources*, 2010, **195**, 2419-2430.